The Astrophysical Journal, 700:1559–1588, 2009 August 1 doi:10.1088/0004-637X/700/2/1559

THE REST-FRAME OPTICAL LUMINOSITY FUNCTION OF CLUSTER GALAXIES AT $z < 0.8$ AND THE ASSEMBLY OF THE CLUSTER RED SEQUENCE*

Gregory Rudnick[1,15], Anja von der Linden[2,16], Roser Pelló[3], Alfonso Aragón-Salamanca[4], Danilo Marchesini[5], Douglas Clowe[6], Gabriella De Lucia[2,17], Claire Halliday[7], Pascale Jablonka[8], Bo Milvang-Jensen[9,10], Bianca Poggianti[11], Roberto Saglia[12], Luc Simard[13], Simon White[2], and Dennis Zaritsky[14]
[1] NOAO, 950 N. Cherry Ave., Tucson, AZ 85719, USA; grudnick@ku.edu
[2] Max-Planck-Institut für Astrophysik, Karl-Schwarzschild-Str. 1, D-85741, Garching, Germany
[3] Laboratoire d'Astrophysique de Toulouse-Tarbes, CNRS, Université de Toulouse, 14 Avenue Edouard Belin, 31400-Toulouse, France
[4] School of Physics and Astronomy, University of Nottingham, University Park, Nottingham NG7 2RD, UK
[5] Astronomy Department, Yale University, P.O. Box 208101, New Haven, CT 06520-8101, USA
[6] Department of Physics & Astronomy, Clippinger Labs 251B, Athens, OH 45701, USA
[7] Osservatorio Astrofisico di Arcetri, Largo E.Fermi, 5. 50125 Florence, Italy
[8] Observatoire de Genève, Laboratoire d'Astrophysique Ecole Polytechnique Federale de Lausanne (EPFL), CH-1290 Sauverny, Switzerland
[9] Dark Cosmology Centre, Niels Bohr Institute, University of Copenhagen, Juliane Maries Vej 30, 2100 Copenhagen Ø, Denmark
[10] The Royal Library/Copenhagen University Library, Research Department, Box 2149, 1016 Copenhagen K, Denmark
[11] Osservatorio Astronomico di Padova, Vicolo dell'Osservatorio 5, 35122 Padova, Italy
[12] Max-Planck Institut fur extraterrestrische Physik, Giessenbachstrasse, D-85748, Garching, Germany
[13] Herzberg Institute of Astrophysics, National Research Council of Canada, Victoria, BC V9E 2E7, Canada
[14] Steward Observatory, University of Arizona, 933 North Cherry Avenue, Tucson, AZ 85721, USA
Received 2008 July 1; accepted 2009 June 2; published 2009 July 15

ABSTRACT

We present the rest-frame optical luminosity function (LF) of red-sequence galaxies in 16 clusters at $0.4 < z < 0.8$ drawn from the ESO Distant Cluster Survey (EDisCS). We compare our clusters to an analogous sample from the Sloan Digital Sky Survey (SDSS) and match the EDisCS clusters to their most likely descendants. We measure all LFs down to $M \sim M^{\star} + (2.5–3.5)$. At $z < 0.8$, the bright end of the LF is consistent with passive evolution but there is a significant buildup of the faint end of the red sequence toward lower redshift. There is a weak dependence of the LF on cluster velocity dispersion for EDisCS but no such dependence for the SDSS clusters. We find tentative evidence that red-sequence galaxies brighter than a threshold magnitude are already in place, and that this threshold evolves to fainter magnitudes toward lower redshifts. We compare the EDisCS LFs with the LF of coeval red-sequence galaxies in the field and find that the bright end of the LFs agree. However, relative to the number of bright red galaxies, the field has more faint red galaxies than clusters at $0.6 < z < 0.8$ but fewer at $0.4 < z < 0.6$, implying differential evolution. We compare the total light in the EDisCS cluster red sequences to the total red-sequence light in our SDSS cluster sample. Clusters at $0.4 < z < 0.8$ must increase their luminosity on the red sequence (and therefore stellar mass in red galaxies) by a factor of 1–3 by $z = 0$. The necessary processes that add mass to the red sequence in clusters predict local clusters that are overluminous as compared to those observed in the SDSS. The predicted cluster luminosities can be reconciled with observed local cluster luminosities by combining multiple previously known effects.

Key words: galaxies: clusters: general – galaxies: evolution – galaxies: formation – galaxies: luminosity function, mass function

Online-only material: color figures

1. INTRODUCTION

Most of the stellar mass in the local universe is contained in "red and dead" galaxies, i.e., galaxies which have stopped forming stars at an appreciable level and whose light is thus dominated by old, red stars (Hogg et al. 2002). To understand how stars form and galaxies are assembled, we therefore need to determine how the red galaxy population evolves through time. Red galaxies are located on a tight sequence in color and magnitude, the "red sequence" (e.g., de Vaucouleurs 1961; Visvanathan & Sandage 1977), and the very small intrinsic scatter in color implies that the red colors result from uniformly old stellar ages (e.g., Bower et al. 1998). Old ages for red-sequence galaxies are also found by studies of their stellar indices (e.g., Trager et al. 1998). Some studies even find a stellar mass dependence in the mean stellar age, such that lower mass galaxies formed their stars at later epochs than those that are more massive (e.g., Thomas et al. 2005), but this result is still controversial as Trager et al. (2008) find no such trend in their studies of Coma cluster early types.

At face value, direct lookback observations may support these local archaeological studies as the total stellar mass on the red sequence may have doubled since $z \sim 1$ (Bell et al. 2004; Faber et al. 2007; Brown et al. 2007). Cimatti et al. (2006) and Brown et al. (2007) concluded that this mass growth comes primarily from the addition of low mass galaxies to the red sequence at late

* Based on observations collected at the European Southern Observatory, Chile, as part of large programme 166.A-0162 (the ESO Distant Cluster Survey).
[15] Department of Physics and Astronomy, Currently at The University of Kansas, Malott room 1082, 1251 Wescoe Hall Drive, Lawrence, KS, 66045, USA.
[16] Currently at Kavli Institute for Particle Astrophysics and Cosmology, Stanford University, 452 Lomita Mall, Stanford, CA 94305-4085, USA.
[17] Currently at INAF, Astronomical Observatory of Trieste, via Tiepolo 11, I-34143 Trieste, Italy.

times, with the most luminous red-sequence galaxies ($L > 4L^{\star}$) appearing to have been in place since $z > 1$. As Trager et al. (2008) point out, however, it may be hard to relate the direct lookback results to studies of local galaxies, as the latter may be susceptible to very small amounts (a few percent) of late star formation.

It is impossible to study the evolution of red galaxies without examining the influence of environment. Going all the way back to Hubble & Humason (1931) it has been known that there are significant correlations between color and environment, star formation rate (SFR) and star formation history (SFH) and environment, and morphology and environment (e.g., Dressler 1980), such that dense environments, e.g., the centers of galaxy clusters, have much higher fractions of red-sequence galaxies than the field. Local studies suggest that luminous ellipticals in galaxy clusters have older stellar ages than those in the field (Thomas et al. 2005) but studies at high redshift detected no difference in the ages of field and cluster elliptical galaxies (van der Wel et al. 2005; van Dokkum & van der Marel 2007). Nonetheless, the large differences between clusters and the field even at intermediate redshift, which are measured in terms of the morphological fraction (e.g., Postman et al. 2005; Smith et al. 2005; Desai et al. 2007) and the fraction of star-forming galaxies (e.g., Poggianti et al. 2006) implies that a galaxy's evolutionary path might be strongly affected by the environment in which it lives as it evolves through cosmic time. Poggianti et al. (2006) postulate that massive ellipticals in clusters may have been formed at high redshift but that lower luminosity red galaxies are added to the cluster at $z < 1$.

From a theoretical standpoint, some models (e.g., De Lucia et al. 2006) predict that stars in red galaxies were formed at high redshift and that the formation epoch of the stars is earlier for higher mass galaxies. It is nonetheless not clear if these models can be reconciled in detail with the observed evolution in the increase of mass on the red sequence at $z < 1$. Also not clear is if the properties of galaxies as a function of environment are being properly treated in some models as none of the commonly implemented processes, e.g., ram-pressure stripping, harassment, strangulation, can reproduce the observed dependence of the red and blue galaxy fraction on, e.g., halo mass and central halo galaxy type at low redshift (e.g., Weinmann et al. 2006) or at $z \sim 1$ (Coil et al. 2008).

One way to study the evolving galaxy population is to use the luminosity function (LF; see Binggeli et al. 1988 for a review), which describes the number of galaxies per unit luminosity. The LF encodes information about the efficiency of star formation and feedback in galaxies and how galaxies populate their parent dark matter halos.

Enabled by large surveys at low redshift such as two-degree field (2dF; Folkes et al. 1999) and the Sloan Digital Sky Survey (SDSS; York et al. 2000) it is now possible to construct the detailed LF of low-redshift galaxies in a range of environments. For example, using the 2dFGRS, De Propris et al. (2003) measured the composite LF in a set of local galaxy clusters and found that the clusters have a brighter characteristic luminosity and a steeper faint-end slope than the field, with the largest difference being found for spectroscopically identified non-star-forming galaxies. The availability of these well characterized local LF determinations provides well established reference points against which we measure evolution in the cluster galaxy population. Simultaneously, the recent availability of deep multicolor photometry of intermediate- and high-redshift clusters with extensive spectroscopic follow-up have allowed the galaxy population to be studied out to $z \sim 1$ in the universe's densest regions.

De Lucia et al. (2004; hereafter DL04) were the first to measure the evolution of the red-sequence LF in clusters at high redshift by studying the ratio of luminous-to-faint red-sequence galaxies $N_{\rm lum}/N_{\rm faint}$ in four clusters at $z \sim 0.7$ drawn from the ESO Distant Cluster Survey (EDisCS). They found that this ratio was significantly higher in the high-redshift clusters than in the Coma cluster. Subsequently, this redshift trend in $N_{\rm lum}/N_{\rm faint}$ was confirmed by Goto et al. (2005) and Tanaka et al. (2005) in a few clusters, and by De Lucia et al. (2007; hereafter DL07), Stott et al. (2007), and Gilbank et al. (2008) in significantly larger samples. Tanaka et al. (2005), DL07, and Gilbank et al. (2008) also found that the evolution of $N_{\rm lum}/N_{\rm faint}$ depends weakly on cluster velocity dispersion and DL07 and Gilbank et al. (2008) found that poorer systems evolve marginally slower than richer systems at $0.4 < z < 0.8$. The behavior in Tanaka et al. (2005) is based on only one cluster and is harder to generalize. Tracing the evolution to $z = 0$, however, there is some disagreement between DL07 and Gilbank et al. (2008). In DL07, it appears that the low-dispersion systems have converged to the $N_{\rm lum}/N_{\rm faint}$ value of the Coma cluster while the high-dispersion systems require significant evolution to reach the value from SDSS or Coma. On the other hand, the poor systems of Gilbank et al. (2008) have systematically higher $N_{\rm lum}/N_{\rm faint}$ values than rich systems at $0.4 < z < 0.6$ and therefore need to evolve more at $z < 0.4$ to come into agreement with the local value. The origin of this apparent discrepancy is hard to track down since DL07 and Gilbank et al. (2008) use different effective velocity dispersion cuts and different magnitude limits defining the split between faint and luminous galaxies. At the same time Andreon (2006, 2008) claim a weak trend in $N_{\rm lum}/N_{\rm faint}$ with redshift and no trend with velocity dispersion. In their Figure 4, however, the amount of redshift evolution appears similar to that from DL07. It is also not easy to compare the trends with velocity dispersion between the two works since the Andreon (2008) sample contains no clusters below 600 km s^{-1}, which comprises a large fraction of the DL07 and Gilbank et al. (2008) samples.

This paper makes a series of advances over previous works by computing the full red-sequence LFs from EDisCS and comparing them to the local red-sequence cluster LF as determined from the SDSS. The EDisCS sample is the largest sample that probes well past $z = 0.5$, all the way out to $z = 0.8$, has deep multiband photometry that enables the construction of rest-frame optical LFs, and has a large range in cluster velocity dispersion. In this paper, we extend the work of DL07 significantly by measuring the nonparametric LF, fitting Schechter functions, and measuring the detailed evolution of red-sequence galaxies. In doing so we pay specific attention to the ability to determine membership from galaxies with only photometry. Our large range in velocity dispersion permits us to study how evolution in the LF depends on velocity dispersion and our deep photometry makes us complete well below $M^{\star}$. We also make the first comparison of the composite cluster red-sequence LF to that in the field and measure their comparative evolution. This test is crucial as it spans the full range of galaxy environment and speaks directly as to whether the cluster and field red galaxy populations are built up at different rates. Finally, we measure the evolution of the total light on the red sequence in clusters and discuss its implications for how mass is added to the cluster red sequence over time. We do not address in detail the total LF or that of blue galaxies as we show in Section 4.5 that LFs from photometric data can only be robustly computed for red galaxies.

In this paper, we examine the rest-frame optical LF of the red galaxies in EDisCS clusters. The rest-frame near-infrared (NIR) LF and stellar mass function will be presented in A. Aragón-Salamanca et al. (2009, in preparation). In Section 2, we discuss the survey strategy and describe the data. In Section 3, we discuss our techniques for determining cluster membership. In Section 4, we describe our estimation of rest-frame luminosities and present our construction of the rest-frame optical LF. We present our results in Section 5, discuss them in Section 6, and summarize and conclude in Section 7. Throughout we assume "concordance" Λ-dominated cosmology with $\Omega_M = 0.3, \Omega_\Lambda = 0.7$, and $H_o = 70h_{70}$ km s^{-1} Mpc^{-1} unless explicitly stated otherwise. All magnitudes are quoted in the AB system.

2. OBSERVATIONS AND DATA

2.1. Observations and Survey Description

The survey strategy and description are presented in detail in White et al. (2005, hereafter W05) who also present the optical photometry and the construction of photometric catalogs. The near-Infrared (NIR) photometry will be presented in (A. Aragón-Salamanca et al. 2009, in preparation). The spectroscopic data are presented in Halliday et al. (2004) for the first five clusters with full spectroscopy and in Milvang-Jensen et al. (2008) for the full EDisCS sample. The survey description and data will be summarized briefly below.

The original goal of EDisCS was to study in detail a set of 10 clusters at $z \sim 0.5$ and 10 at $z \sim 0.8$. Our survey draws on the optically selected sample of clusters from the LCDCS (Gonzalez et al. 2001). After confirming the presence of a galaxy surface overdensity at the expected position and the presence of a red sequence using short images with the FORS2 instrument on the VLT, we initiated deep imaging of 10 clusters in each redshift bin. We observed every field in either the *B*-, *V*-, *I*-, and K_s bands or in the *V*-, *R*-, *I*-, *J*-, and K_s bands depending on whether the LCDCS redshift estimate of the cluster was at 0.5 or 0.8, respectively. The optical data were all obtained with FORS2/VLT and the NIR data were obtained with the SOFI instrument on the NTT.

From the first reduction of our imaging data we computed photometric redshifts to get a more precise redshift estimate for the clusters (Pelló et al. 2009). These redshifts were used to target objects for spectroscopic observations with FORS2/VLT. Now complete, our extensive spectroscopic observations consist of high signal-to-noise (S/N) data for $\sim$ 30–50 members per cluster and a comparable number of field galaxies in each field down to $I \sim 22$. As explained in W05, deep spectroscopy was not obtained for two of the EDisCS fields (CL1122.9-1136 and CL1238.5-1144), the former of which showed no evidence for a cluster in the initial, shallow spectroscopic observations. These clusters will not be used in this study, leaving 18 of which one (CL1119.3-1129) does not have any NIR data.

2.2. Catalog Construction and Total Flux Measurements

We measured two types of magnitudes for our galaxies, matched aperture magnitudes and SExtractor AUTO magnitudes. The former are used for measuring colors and the spectral energy distributions (SEDs) used to fit the photometric redshifts. The latter are used to estimate the total magnitude of the galaxies in question. We describe each in turn. All magnitudes have been corrected for galactic extinction from Schlegel et al. (1998).

Before the measurement of matched aperture fluxes, all images with seeing better than FWHM = 0.″8 were convolved to FWHM = 0.″8. The seeing across all bands ranged from 0.″6 to 1.″0 with most observations having FWHM $\leqslant$ 0.″8.

Flux catalogs were created using the SExtractor software (Bertin & Arnouts 1996) in the two image mode, detecting in the unconvolved (i.e., natural seeing) *I*-band image and measuring fluxes in matching apertures in all other bands. Colors were measured with the same aperture in all bands, using either isophotal apertures defined from the detection images for those galaxies that were not crowded or using circular apertures with $r = 1.''0$ for those galaxies that were crowded. With this dual choice of matched apertures we obtained a high-S/N measurement of the color while minimizing the biases due to neighboring objects.

Obtaining accurate total magnitudes is important when characterizing the LF. A true total magnitude estimate is not possible, however, due to uncertainties in the galaxy profile at large radii coupled with an uncertain knowledge of the sky level. As described in W05, therefore, we attempted to measure pseudo-total magnitudes (called "total" magnitudes throughout) in the *I*band using the AUTO magnitude from SExtractor. These magnitudes were measured on the images at their natural seeing. The SExtractor AUTO measurement is executed within a Kron-like aperture (Kron 1980) and measures the flux within a radius corresponding to two times the first moment of the light distribution. The AUTO magnitudes for each object have a minimum aperture radius of 3.5 pixels (or 0.″7). The AUTO aperture is quite large for bright objects but for faint objects the AUTO aperture shrinks its size to the minimum allowable limit. In this regime, light will be lost out of the aperture even for point sources, since the stellar point spread function (PSF) throws significant amounts of light beyond this minimum aperture. Such an effect was also noted in the absolute magnitude estimates of Labbé et al. (2003) and we adopt their approach for correcting for this effect, which we summarize here. Correcting for this offset explicitly is difficult because we do not know the intrinsic profile of the galaxies whose photometry we wish to measure. However, a conservative and necessary correction can be made by accounting for the light that would be missed assuming that the object is a point source. While the amount of light lost may be larger for extended objects, this robust correction must be made regardless of the intrinsic object shape. Since we only define the total magnitude consistently from the *I*-band image, and use this to scale our rest-frame luminosities (as measured in the matched apertures) to total luminosities, we only calculated the aperture correction for the *I*-band image. This neglects the effects of large color gradients, but the resultant error in the total magnitudes should not dominate our uncertainties. We determined an empirical stellar curve of growth for each image using a set of bright, unsaturated, and isolated stars. Using the curve of growth, we computed the correction as a function of AUTO aperture area and apply it to the AUTO magnitudes. The corrected magnitudes become our "total" magnitudes, $I_{\rm tot}$. For the two clusters with the worst and best seeing in the *I* band we plot the dependence of these corrections and the AUTO aperture size on the $I_{\rm tot}$ in Figure 1. The corrections range from median values of $\sim$ 0.04 mag at $20.4 < I_{\rm tot} < 22.4$ to $\sim$ 0.09 mag at $24.4 < I_{\rm tot} < 24.9$.

To check how well this aperture correction does in retrieving the true total magnitude, we compared the $I_{\rm tot}$ values to those derived from two-dimensional (2D) profile fits to the *I*-band data using the GIM2D software (Simard et al. 2002; Simard et al.

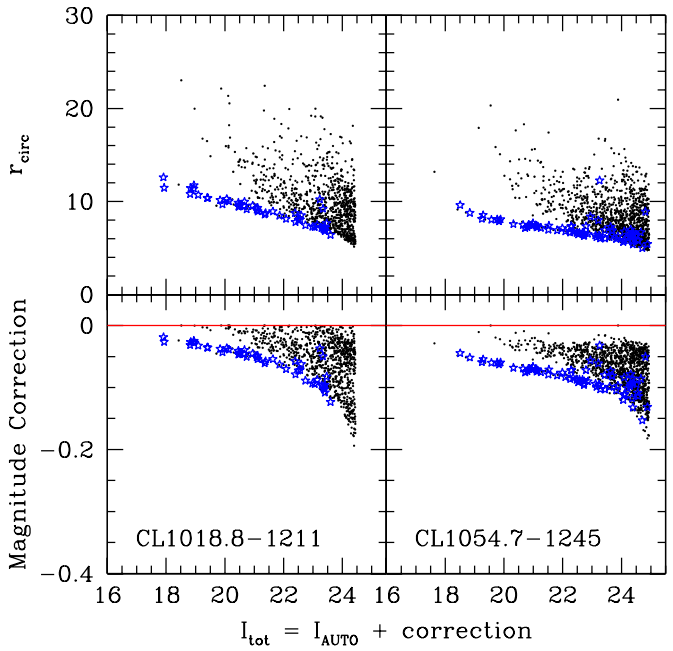

Figure 1. Illustration of how our aperture correction depends on apparent magnitude for two clusters with the worst and best *I*-band image quality in our sample, CL1018.8-1211 and CL1054.7-1245, respectively. The *x*-axis in all plot is our "total" estimate of the *I*-band magnitude, I_{tot}, which is the AUTO *I*-band magnitude with a point source aperture correction. The bottom row of panels shows how the correction depends on I_{tot} and the top panel shows how the circularized AUTO aperture radius depends on I_{tot}. Only objects with no evidence of crowding have been used. Stars are indicated by blue stars. At every magnitude, the objects with the smallest apertures receive the largest correction. The smallest apertures correspond to those for stars.

(A color version of this figure is available in the online journal.)

2009). We fit bulge+disk models to the galaxies and extrapolated the profiles to get total magnitude estimates I_{GIM2D}. For sources with no nearby neighbors, I_{GIM2D} should be relatively free of bias (Häußler et al. 2007). At $20.4 < I_{tot} < 22.4$ and $22.4 < I_{tot} < 24.4$ we find a median difference $I_{tot} - I_{GIM2D}$ of 0.02–0.04 and 0.06–0.1 respectively, such that I_{GIM2D} is systematically brighter. However, in Simard et al. (2002) those authors used extensive simulations to show that the GIM2D magnitudes are biased brighter by the same order as our measured difference between I_{tot} and I_{GIM2D}, implying that our I_{tot} magnitudes indeed are good approximations to the true total magnitude.

We have verified that our results do not depend sensitively on the value of the correction, as it only significantly effects the very faintest galaxies in the sample, which do not dominate any of the observed effects.

3. DETERMINING CLUSTER MEMBERSHIP

At intermediate redshift, the contrast of a cluster against the background and foreground is very low and an estimation of the cluster galaxy LF necessitates that a sample of cluster members be assembled which has been cleaned of foreground and background interlopers. Spectroscopy is obviously the most accurate method of accomplishing this and spectroscopic redshifts can be determined for single objects down to $I \sim 24.5$ with the use of 8 m class telescopes. Nonetheless, determining redshifts for large numbers of cluster members in multiple clusters, even with large time allocations on 8 m class telescopes, is limited to relatively bright magnitudes, e.g., $I \lesssim$ 22–23 (Tran et al. 2007; Halliday et al. 2004). To determine the cluster membership for magnitude-selected samples down to $I \sim 25$ it is therefore necessary to use alternate techniques. We have employed two methods to accomplish this, one based on photometric redshifts z_{phot} and the other based on statistical background subtraction. These membership techniques have also been used in previous works on the EDisCS clusters, e.g., DL07, DL07. LFs computed from photometric redshifts and statistical background subtraction will hereafter be referred to as LF_{zp} and LF_{ss}, respectively. We discuss these two methods in this section, while in Section 4.5 we compare LF_{zp} and LF_{ss} to determine the robustness of our results.

3.1. Photometric Redshifts

In general, photometric redshift techniques estimate the redshift of a galaxy by modeling the broadband SED with a set of template spectra (e.g., Fernández-Soto et al. 1999; Rudnick et al. 2001). The resulting χ^2 of the template fit as a function of redshift gives an estimate of the redshift probability distribution $P(z)$ and hence the most likely redshift. As an example application of photometric redshift techniques to cluster studies, Toft et al. (2004) used their z_{phot} estimates to determine membership by taking a very wide $\Delta z = \pm 0.3$ slice in redshift and selected every galaxy within this slice as being a cluster member. A slice of this width, however, is $\sim$ 100 times larger in velocity than the expected velocity width of the cluster, implying a large contamination from field galaxies. Also, the performance of photometric redshifts is expected to depend on the galaxy SED shape, e.g., blue star-forming galaxies have weak Balmer/4000 Å breaks which result in weaker photometric redshift constraints and possible larger systematic errors. This color dependence on the z_{phot} accuracy can only be quantified by using a large number of spectroscopic redshifts that span a large range of SED shape/color in the desired redshift range, preferably with identical photometry. Until now, such large spectroscopic samples in intermediate-redshift cluster fields have not been available.

We explore an alternative photometric-redshift-based interloper subtraction technique with EDisCS, which tries to mitigate the disadvantages mentioned above. The photometric redshifts for the EDisCS sample, their performance, and their use to isolate cluster members, are described in detail in Pelló et al. (2009). Here we provide a brief summary.

Photometric redshifts were computed for every object in the EDisCS fields using two independent codes, a modified version of the publicly available Hyperz code (Bolzonella et al. 2000) and the code of Rudnick et al. (2001) with the modifications presented in Rudnick et al. (2003). The accuracy of both methods is $\sigma(\delta z) \approx 0.05$–$0.06$, where $\delta z = \frac{z_{spec} - z_{phot}}{1+z_{spec}}$. By fitting stellar templates to the observed SEDs of stars we searched for zero-point offsets and found no offsets except for a small one in the *B* band of CL1353.0-1137. We applied the offset for this one band when performing the photometric redshift fits. We established membership using a modified version of the technique first developed in Brunner & Lubin (2000), in which $P(z)$ is integrated in a slice around the cluster redshift for the two codes. The width of the slice around which $P(z)$ is integrated should be on the order of the uncertainty in redshift for the galaxies in question. In our case we use a $\Delta z = \pm 0.1$ slice around the spectroscopic redshift of the cluster z_{clust}. We reject a galaxy from our membership list if $P_{clust} < P_{thresh}$ for either code. We calibrate P_{thresh} from our $\sim$ 1900 spectroscopic redshifts. Our values of P_{thresh} were chosen to maximize the efficiency with which we can

reject spectroscopic nonmembers (down to $I = 22$) while retaining at least $\approx 90\%$ of the confirmed cluster members, independent of their rest-frame $(B - V)$ color or observed $(V - I)$ color. In practice we were able to choose thresholds such that we satisfied this criterion while rejecting 45%–70% of spectroscopically confirmed nonmembers. Applied to the entire magnitude-limited sample, our thresholds reject 75%–93% of all galaxies with $I_{\rm tot} < 24.9$. It is worth noting that it is very difficult to assess our absolute contamination for two reasons. First, even the extensive spectroscopy we currently have was performed on a subsample of the photometric catalog that was designed to exclude objects with an extremely low probability of being at the cluster redshift. Any estimates based on this spectroscopy may therefore not be entirely indicative of the true contamination down to the spectroscopic completeness limit. Second, we do not have spectroscopy for galaxies down to the faint limit of the photometric catalog and it becomes impossible to definitively measure the contamination at these faint magnitudes without significantly deeper spectroscopy or highly model-dependent assumptions.

Our method establishes cluster membership using a redshift interval smaller than that employed in other photometric-based membership techniques (e.g., Toft et al. 2004) and therefore should suffer considerably lower field contamination. As a check of how much more contamination we would have if we adopted the technique of Toft et al. (2004) we have remeasured our membership requiring that each galaxy be within $\Delta z = \pm 0.3$ of the cluster redshift. The number of cluster members with this technique is typically 2–3 times larger than when using our membership technique, implying a correspondingly larger contamination.

Despite the apparently good performance of the photometric redshift technique, the $z_{\rm phot}$ estimates are only well tested at relatively bright magnitudes, e.g., $I \lesssim 22$. Because the $z_{\rm phot}$-based membership technique is largely untested at $I \gtrsim 22$, it will be difficult to trust the faint-end slope of the LF derived from such techniques. For this reason, it is desirable to use complementary photometric methods to establish membership.

3.2. Statistical Background Subtraction

An independent method of establishing cluster membership is the statistical subtraction technique (e.g., Aragón-Salamanca et al. 1993; Stanford et al. 1998). In this technique, number counts in the cluster field are compared to those in an "empty" field and the excess counts are used to assign a membership probability to each galaxy in the cluster field. This method becomes increasingly inefficient at high redshift, where the contrast of the cluster against the background becomes increasingly low. In addition, this method provides no membership probability for individual galaxies, but rather gives every galaxy in a given region of magnitude (and color) space an identical probability. At the same time, it suffers from completely different uncertainties than the photometric redshift technique and is a useful complement to judge the robustness of our results.

Ideally, the comparison catalog used to create the field counts should contain the same bands as used in the cluster fields and cover a large enough area to minimize cosmic variance. For our statistical-background-subtraction-based membership we utilized a "field" catalog from the Canada France Deep Field (CFDF; McCracken et al. 2001).[18] This field has the advantages of having matched aperture photometry in *V*- and *I* bands and AUTO magnitudes in the *I* filter, while also covering 0.25 deg^2, roughly 20 times the area of the optical coverage in an individual EDisCS field. The depth of the CFDF is only $I = 24.5$ and so all LFs computed via statistical background subtraction will be limited to $I < 24.5$. The CFDF is the only publicly available field that satisfies our requirements for a background field. These were (1) that it must have photometry in at least V and I since these filters are in common for both the EDisCS filter sets (*BVIK* and *VRIJK*) and (2) that it must have a large enough area to overcome the effects of cosmic variance in the background subtraction estimate. While there are other fields with deep multifield photometry over a moderate area (e.g., Chandra Deep Field South (CDF-S), NOAO Deep Wide-Field Survey (NDWFS)), there are no publicly available surveys with both deep *V* and *I* at a depth comparable to EDisCS and with large enough area to overcome cosmic variance. For example, The CDF-S that was targeted by the FIREWORKS survey (Wuyts et al. 2008) is known to be underdense at $z \sim 0.7$ compared to the much larger Extended CDF-S (ECDF-S; Taylor et al. 2009) and so is not a good sample of the mean background. Also, the NDWFS (Brown et al. 2007), which we use in Section 6.2 has no *V* filter and a very wide *B*-band filter (essentially $U + B$), which makes it impossible to use as a background field for the EDisCS clusters with only *BVIK* photometry.

We use a method similar to the one presented by Pimbblet et al. (2002) and refer to that paper for details, although we summarize it briefly here. We bin the CFDF data and our own in observed $(V - I)$ color and $I_{\rm AUTO}$ using bins of 0.5 in color and magnitude (using color bins of 0.3 results in nearly identical LFs). Note that we do not use $I_{\rm tot}$ when performing the statistical subtraction, as the CFDF does not have aperture-corrected magnitudes. We assume that the AUTO magnitudes perform similarly for both surveys. In a given bin we scale the number of field galaxies to the area of the cluster under consideration to derive the number of expected field galaxies. We first retain all spectroscopically confirmed members and exclude all spectroscopically confirmed nonmembers. Then we subtract off a random subset of the remaining galaxies equal in number to the expected number of field galaxies (minus the number of spectroscopically confirmed nonmembers) to obtain a realization of the cluster member population. In bins where the number of expected field galaxies are greater than the number of member candidates, we merge adjacent bins in color until the number of expected field galaxies is greater than or equal to the number of member candidates in the expanded bin. This is analogous to expanding the bins until the membership probabilities again lie between 0 and 1. As explained in Appendix A of Pimbblet et al. (2002) this method has an advantage over similar methods in that it preserves the original probability distribution, albeit smoothed over larger scales.

The moderately large area of the CFDF gives an accurate representation of the mean density of field galaxies but on spatial scales similar to that of our clusters the number counts of field galaxies may vary and the true underlying field may be systematically different from the mean. We use the entire CFDF area to calculate our best estimate of the membership sample for each cluster. When calculating the uncertainty in the cluster membership, we split the CFDF into tiles, with each tile having the same area as the area of the cluster under consideration. In practice, this resulted in greater than 20 independent tiles in the CFDF. We then performed 100 Monte Carlo iterations of the

[18] This catalog has been kindly provided to use by H. McCracken.

subtraction, where each iteration uses a randomly chosen tile to derive the expected field population.

4. MEASURING THE LUMINOSITY FUNCTION

In this section, we will present our method for determining rest-frame luminosities, for measuring the LF of cluster galaxies as a whole and split by color, and for fitting Schechter (1976) functions to the measured LFs. We will present a comparison of LF_{zp} and LF_{ss} and discuss why robust LF determination of cluster galaxies can only be made for the red galaxy population.

4.1. Determining Rest-frame Luminosities

Rest-frame luminosities $L_{\lambda}^{\rm rest}$ and rest-frame colors were calculated using the technique described in Rudnick et al. (2003) and assuming that every galaxy selected as a cluster member has $z = z_{\rm clust}$. Our $L_{\lambda}^{\rm rest}$ estimates were computed from the matched aperture magnitudes (see Section 2.2), which almost certainly miss flux compared to the $I_{\rm tot}$ estimate. To scale our $L_{\lambda}^{\rm rest}$ estimates to total values we therefore multiply every $L_{\lambda}^{\rm rest}$ value by the ratio of the total I-band flux to that in the I-band-matched aperture. The median correction ranges from a few percents at $I_{\rm tot} \sim 20$–21 to $\sim 30\%$–50% at $I_{\rm tot} \sim 24.4$–24.9.

Which rest-frame luminosities we are able to use depends on which technique we employ to determine cluster membership. For the photometric redshift method the full range of rest-frame wavelengths are available, as the probability of each galaxy residing at the cluster redshift is computed directly from its SED. Therefore, the SED is by definition consistent with being at (or near) the cluster redshift and any interpolation between the observed bands based on the templates at that redshift should yield a robust estimate of $L_{\lambda}^{\rm rest}$. We therefore can compute rest-frame magnitudes of cluster members in many rest-frame bands spanned by our observed filter sets, e.g., $g_{\rm rest}$, $r_{\rm rest}$, and $i_{\rm rest}$. The rest-frame NIR LFs will be presented in A. Aragón-Salamanca et al. (2009, in preparation).

The statistical background subtraction method, however, limits the rest-frame wavelengths for which luminosities can be robustly computed to those that are straddled by the observed subtraction filters. The reasoning is as follows. Recall that the photometric redshift technique uses the full SED information to determine membership on an individual basis. With statistical subtraction, however, the membership probability is not known for each galaxy, but rather for all galaxies in a region of color–magnitude space based on their relative numbers with respect to those in an empty field image. This implies that some fraction of the galaxies classified as members will actually be at different redshifts than the cluster. For rest-frame wavelengths straddled by the observed subtraction bands (in our case $\lambda_V < (1 + z_{\rm clust}) \times \lambda_{\rm rest} < \lambda_I$) this is not a problem, as the color of every candidate member is constrained to be similar to that of the very cluster galaxies that cause the overdensity in counts in that color–magnitude bin, regardless of whether or not that candidate truly is a member. Therefore, the use of templates at $z_{\rm clust}$ can be used to determine $L_{\lambda}^{\rm rest}$ without large systematic errors if the galaxy is truly a nonmember. However, this statistical subtraction method does not insist that the SED of the galaxy outside of the observed subtraction bands is consistent with one at the cluster redshift. For this reason, rest-frame wavelengths outside the subtraction bands will be subject to uncertain extrapolations and will not be robust. For clusters at our redshift, the condition $\lambda_V < (1 + z_{\rm clust}) \times \lambda_{\rm rest} < \lambda_I$ is approximately satisfied for the $g_{\rm rest}$- and $B_{\rm rest}$ bands, which we limit ourselves to for LFs computed with statistical subtraction.

4.2. A Nonparametric Estimate of the LF

We first measure the LF of every cluster by simply binning the sample into absolute magnitudes and counting the number of galaxies in each bin. As is done in previous works, we exclude the Brightest Cluster Galaxy (BCG) and galaxies brighter than the BCG from the LF computation. The properties of the EDisCS BCGs haven been presented separately in Whiley et al. (2008).

For LF_{zp} the error bars in each bin represent the Poisson errors on the retained galaxies, computed using the formulae of Gehrels (1986). For LF_{ss} the best-fit LF is that derived using the subtraction over the whole CFDF. There are two sources of error that contribute to LF_{ss}. The first source is the Poisson error on the number of galaxies in each cluster field retained as members. The second source of error originates in the uncertain background measurement, which we determine using Monte Carlo realizations for small subtiles of the CFDF in estimating the field (see Section 3.2). In this case, we computed the LF for each Monte Carlo realization of the subtraction and took the 68% confidence intervals of the resultant LFs as an estimate of the error. This error was then added in quadrature to the Poisson error to achieve a total error.

In constructing the LF for each cluster there are two issues to consider, the detection limit in observed total magnitudes and the corresponding limit in absolute magnitude. As described in W05, we establish our completeness in the observed I-band magnitude in an empirical way by comparing our number counts to those from much deeper surveys (see W05, Figure 1). There is ample evidence that the intrinsic slope of the I-band number counts is a rising power law at faint magnitudes (e.g., Metcalfe et al. 2001; Heidt et al. 2003) and we define our completeness as the magnitude at which our observed number counts in total magnitudes deviate from a power law defined by the deeper observations. There are two reasons this is reasonable. First, the number counts contributed by the cluster at faint magnitudes are much smaller than the contribution by the field. This is evidenced by the fact that 80%–90% of galaxies are rejected by statistical subtraction at $I_{\rm tot} < 24.9$ (Pelló et al. 2009). Also, the slope of our number counts is parallel to that from deeper fields at $22 < I_{\rm tot} < 24$ for the high-z clusters and $23 < I_{\rm tot} < 24$ for the low-z clusters, where we expect the cluster to no longer contribute significantly to the counts. For this reason, we feel that our faint counts can directly be compared to that of the field. Second, our total magnitudes (which include an aperture correction) result in a rapid drop-off in the number counts at faint magnitudes. This is not seen in surveys that measure magnitudes without an aperture correction but is a direct result that we count for a minimal amount of missing flux in our faintest galaxies (see Labbé et al. (2003) for a more detailed explanation). Labbé et al. (2003) also showed that a limit defined in this way corresponds to a near perfect detection probability. Because this is a rather conservative estimate of our completeness the S/N is still high (typically > 10; W05) all the way down to our detection limit, allowing the robust computation of magnitudes and colors.

Once we have established our completeness limit in observed magnitude we translate this, for every rest-frame filter, into an absolute magnitude limit that is the most conservative (i.e., brightest) given the whole range of possible galaxy SEDs. If a redshifted rest-frame filter for a given cluster redshift is blueward of the observed I band the brightest limit corresponds to that computed using a 10 Myr old single age population with

solar metallicity and a Salpeter (1955) IMF. This is perhaps overly conservative for red galaxies, but results in the most conservative limit for the whole catalog, so that we are equally complete at all galaxy colors. For redshifted rest-frame filters redward of the observed *I* band we used Elliptical template from Coleman et al. (1980).

We also created composite LFs for subsamples split by redshift and cluster velocity dispersion. We created the composite and its error using the method of Colless (1989), which was also discussed in detail in Popesso et al. (2005). With this method, the composite LF at every magnitude represents the mean fraction of galaxies compared to the number in a normalization region. We choose the normalization region to be all magnitudes brighter than the brightest completeness limit that all clusters in that subsample have in common.

When creating the composite clusters, we correct them for passive evolution to the mean redshift for that subsample. As we will describe in subsequent sections, only the LF for red cluster galaxies can be robustly determined and we concentrate mostly on those for the rest of the paper. DL07 showed that the colors of the red sequence can be well fitted by a passively evolving model with $z_{\rm form} \sim 2$–3. We correct the rest-frame magnitudes using a $z_{\rm form} = 2$ single stellar population (SSP) Bruzual & Charlot (2003; hereafter BC03) model with $Z = 2.5\,Z_{\odot}$. In practice, this small evolution correction does not change the binned LF with respect to that computed with no correction. This is because the amount of evolution from each cluster to the center of its redshift bin is significantly smaller than the 0.5 mag bin size used in constructing the LF. For the same reason the exact choice of model used makes little difference in the resulting composite LF.

We compute the LF in two different physical radii, $r < 0.75$ Mpc and $r < 0.5\,R_{200}$, where R_{200} is defined as the radius within which the density is 200 times the critical density:

$$R_{200} = 1.73 \frac{\sigma}{1000\ \mathrm{km\ s^{-1}}} \frac{1}{\sqrt{\Omega_\Lambda + \Omega_0 (1+z)^3}}\, h_{100}^{-1}\ \mathrm{Mpc}, \quad (1)$$

where σ is the cluster velocity dispersion (Finn et al. 2005). The area defined by these two radii is entirely contained within the EDisCS fields for all but one of our clusters (CL1227.9-1138) for which we take only the inscribed area into account when performing the statistical subtraction.[19] For this cluster the lack of data for $\sim 50\%$ of the galaxies within $0.5\,R_{200}$ and $\sim 60\%$ within 0.75 Mpc should not bias the values of $M^\star$ but will result in a larger error bar on that value. For only two of the most massive clusters, CL1216.8-1201 and CL1232.5-1250, is $0.5R_{200}$ larger than 0.75 Mpc. Our conclusions are insensitive to the exact choice of radii and unless otherwise stated we will use $r < 0.75$ Mpc as it is most always the larger of the two and hence will produce the highest S/N LF.

4.3. Schechter Function Fits

We fit Schechter (1976) functions to the binned LFs in each cluster. To fit we created a coarse grid in the three fitted parameters, i.e., $\phi^\star$, $M^\star$, and α. We calculated the χ^2 value at each grid point and took the best-fit solution as an initial guess for the parameters. We then refit the parameters with a narrower range and a finer sampling in the parameter space. We determined the formal uncertainty on each parameter by first converting the χ^2 at each grid point into a probability via $P_{\phi^\star,M^\star,\alpha} = e^{-\chi^2/2}$ and then by marginalizing the probability along the other two parameters to obtain a probability distribution for the parameter in question. We then measured the limits in this parameter that enclosed 68% of the probability as the 1σ formal error bar.

To assess the reliability of such fits we created a set of mock binned LFs by randomly drawing from a set of input values, i.e., the number of galaxies, $M^\star$and α. The errors on each mock LF were Poisson errors on the number of galaxies in each bin. For a given set of parameters we created 100 mock realizations of that LF and fit each realization using the procedure above, and over the absolute magnitude range present in our data. While all three Schechter parameters are highly degenerate, we found that the most poorly constrained parameter was α followed by $M^\star$. The ability to retrieve the parameters was also dependent on the input value of α, since steeper (more negative) α values produced more biased answers. For the red galaxies to which we limit our analyses (see the subsequent sections) $\alpha > -0.6$ and the bias produced by a steep slope is not severe. Nonetheless, through these simulations we found that it was impossible to constrain all three parameters simultaneously using the data from an individual cluster, or even from a composite LF of only a few clusters. We did find however, that we could constrain all three simultaneously if we fit an LF with characteristics akin to the composite LF of the entire EDisCS sample, split into two bins of redshift. We therefore derive α and its uncertainty for the entire EDisCS sample for each band in each redshift bin and use that α when fitting the individual and stacked LFs when split by velocity dispersion. Even when fitting to the whole sample, however, the uncertainties on α are non-negligible. To account for this uncertainty in the fitting of individual clusters or subsamples of the EDisCS clusters, we fit the Schechter function to the data 100 times, with α fixed each time but drawn randomly from a Gaussian with a mean and sigma taken from the fit to the total stacked cluster sample. The 68% confidence interval in the distribution of $M^\star$ from these 100 iterations was then added in quadrature to the formal uncertainties, derived with a fixed α, to derive the total uncertainty in $M^\star$. This may overestimate the error in $M^\star$ as it includes some of the sampling error twice.

4.4. Splitting LFs by color

We divide our sample by $(V - I)$ color into red-sequence galaxies and bluer galaxies. For each cluster we fit the zero point of the color–magnitude relation (CMR) in $(V - I)$ assuming a fixed slope of -0.09 and using the outlier resistant Biweight estimator (Beers et al. 1990) for the zero point. In performing the fit we only use spectroscopically confirmed cluster members with no emission lines. This was the same method as used by DL07. We give the best-fit zero points in Table 1 for the 16 clusters for which a robust LF determination is possible (see Section 5).[20] A relatively constant slope of the CMR can be understood if the slope is primarily a result of a metallicity trend with magnitude (e.g., Kodama & Arimoto 1997) among galaxies with a uniformly old age (Bower et al. 1992), at least among bright galaxies. As shown in, e.g., Kodama & Arimoto

[19] Using the EDisCS data it was realized that the LCDCS BCG candidate for CL1227.9-1138 was not the actual BCG. The true BCG is located significantly offcenter in our FORS data, resulting in the loss of area.

[20] Our values are given at $I_{\rm tot} = 0$ whereas those from DL07 were given at an apparent magnitude that corresponds to $M_V = -20$ when evolution corrected to $z = 0$. DL07 also use Vega magnitudes.

Table 1
Zero points of Fits to Red Sequence

Cluster	z	$ZP_{V-I;I}$ (mag)	σ_{ZP} (mag)
CL1018.8-1211	0.47	3.45	0.10
CL1037.9-1243	0.58	3.65	0.08
CL1040.7-1155	0.70	3.81	0.09
CL1054.4-1146	0.70	3.86	0.06
CL1054.7-1245	0.75	4.08	0.11
CL1059.2-1253	0.46	3.42	0.07
CL1138.2-1133	0.48	3.44	0.11
CL1202.7-1224	0.42	3.34	0.08
CL1216.8-1201	0.79	4.00	0.11
CL1227.9-1138	0.64	3.77	0.06
CL1232.5-1250	0.54	3.58	0.16
CL1301.7-1139	0.48	3.49	0.12
CL1353.0-1137	0.59	3.67	0.12
CL1354.2-1230	0.76	4.03	0.02
CL1411.1-1148	0.52	3.50	0.15
CL1420.3-1236	0.50	3.51	0.09

Notes. Zero points of $V-I$ vs. I_{tot} color–magnitude relation are calculated for spectroscopically defined non-star-forming galaxies. These are defined where $I_{tot}= 0$, which differs from the definition of De Lucia et al. (2007).

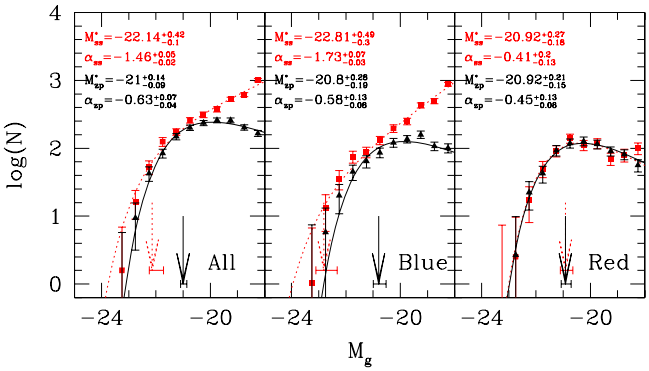

Figure 2. g_{rest}-band composite LFs of EDisCS cluster galaxies. The left panel is for all galaxies, regardless of color. The middle panel is for blue galaxies and the right panel is for red galaxies (see text for definition of colors). The squares show the LF determined using statistical subtraction LF_{ss} and the triangles show the LF determined using photometric redshifts LF_{zp}. The solid and dotted curves show the best-fit Schechter function fits to LF_{zp} and LF_{ss} respectively and the vertical arrows of the same line type show the corresponding best-fit values of $M^{\star}$. The horizontal error bars at the base of the arrows give the 68% confidence limits in $M^{\star}$. When including all galaxies LF_{ss} has a steeper faint-end slope and a larger number of bright galaxies than LF_{zp}. These difference can be traced to the blue galaxies. Both techniques give identical results for the red galaxies.
(A color version of this figure is available in the online journal.)

(1997) and Bower et al. (1998), the rate of change of color with time is insensitive to metallicity, so using the local value for the CMR slope with our intermediate-redshift clusters is a reasonable assumption. As in DL07, we select red-sequence galaxies as those within ±0.3 mag of the best-fit CMR. This is a compromise between the completeness and purity of our red-sequence sample. By allowing our color cut to extend below the CMR, we ensure that we do not miss red galaxies that are slightly bluer than the CMR, but also increase the possibility that there may be some blue galaxy contamination at fainter magnitudes where our photometric errors increase. We used two methods to test how sensitive our results were to the exact form of our red sequence selection. First, we varied the width of our selection slice by ±0.05 mag. This corresponds to the ≈ 0.1 mag error in $(V-I)$ for galaxies at the EDisCS magnitude limit (White et al. 2005). Second, we selected all galaxies redward of the CMR and then reflected them across the CMR. This latter method is similar to what is used by Gilbank et al. (2008) and ensures high sample purity at the risk of missing intrinsically bluer/younger galaxies still formally on the red sequence. In all cases, we find that the LFs with these different methods are consistent to within 1σ, indicating that our results are robust against variations in the red-sequence selection. We believe that this must be partly true due to our conservative magnitude limit and extremely deep VLT photometry.

For each of the samples split by color we compute the individual and composite LFs as described above. As shown in DL04 and DL07, it is also important when establishing the effective magnitude limit on the red sequence to take into account that the S/N of the color measurement of galaxies becomes worse for redder galaxies at a fixed I_{tot} (see Figure 1 of DL07). We take this into account when determining our completeness limit and find that we may miss some red-sequence galaxies in the $24.4 < I < 24.9$ mag bin. Although our LF_{zp} estimates for the high-z clusters are computed to $I = 24.9$, all of the trends described in this paper are completely dominated by effects in the bins at $I < 24.4$. We therefore do not worry about this minor incompleteness in our last bin.

4.5. A Comparison Between Methods

We assess the robustness of our LFs by comparing LF_{zp} and LF_{ss}. In Figure 2, we show the composite LF of all EDisCS clusters as computed with the two methods. The LF_{ss} of all galaxies has a steeper faint-end slope and an overabundance of bright galaxies compared to LF_{zp}. This same behavior is apparent, albeit at lower significance, in all the composite and individual LFs. We also compute the LFs separately for blue and red galaxies and plot these in the middle and right panels of Figure 2, respectively. It is obvious from this figure that the discrepancy only exists for the blue galaxies. In contrast, LF_{ss} and LF_{zp} agree completely for red galaxies, as was found in DL07.

There are at least two possible reasons for the large difference in the faint-end slope between the two techniques that only manifests itself for blue galaxies. First, the effectiveness of LF_{ss} is critically dependent on the validity of the field counts used to make the statistical subtraction. The faint-end slope of the blue number counts is in general steep (e.g., Koo 1986) and we have checked that the faint-end slope of the counts in the CFDF is significantly steeper for blue than for red galaxies. Because the faint-end slope of the blue galaxy counts is so steep, the faint-end slope of the cluster LF is critically dependent on the exact value of the slope. Specifically, the faint-end slope of the counts in the comparison field needs to be the same as the faint-end slope of the counts for field galaxies in the cluster field. If there are slight differences in the way that magnitudes are measured between the field and cluster catalogs, an incorrect faint-end cluster LF can be measured. Indeed, although AUTO magnitudes are used for both the cluster and CFDF catalogs the seeing of the CFDF catalog is ∼ 1.5–2 times worse than that of the EDisCS catalogs and there has been no attempt to match SExtractor catalog parameters. As a result, magnitude-dependent differences in the AUTO magnitudes could be present between the two catalogs and this could cause the very steep faint-end slope of LF_{ss} for blue galaxies. We have checked that a magnitude-independent change in the CFDF magnitudes of up to 0.2 mag has no appreciable effect on the faint-end slope but have not explored more complicated magnitude dependent

effects. We conclude that differences in the way the two surveys measure magnitudes makes it difficult to measure the faint-end LF_{ss} for blue galaxies, where the magnitude measurement of faint galaxies is so crucial. In contrast, the faint-end slope of the number of red galaxies in the CFDF is much shallower than for the blue galaxies and small errors in the magnitude measurements for red galaxies will therefore result in smaller errors in the LF.

Another possible reason for the difference between LF_{ss} and LF_{zp} for blue galaxies, specifically the large difference in the faint-end slope, may come from limitations in the photometric redshift techniques. For the spectroscopic sample we verified that the photometric redshifts performed similarly for red and blue galaxies. Unfortunately given the spectroscopic magnitude limit, we were not able to verify how the photometric redshifts performed at faint magnitudes. In general, the performance of photometric redshift codes depends on the S/N of the flux measurements since a higher S/N measurement allows for a better localization of the features (e.g., the 4000 Å break) used to determine the redshift. For galaxies with weaker intrinsic features in their SEDs, e.g., blue galaxies, the photometric S/N must be higher to yield a comparable redshift accuracy as for galaxies with stronger features, e.g., red galaxies with strong 4000 Å breaks. Since we determine the cluster membership by integrating $P(z)$, a poorer constraint on z_{phot} with a correspondingly broader $P(z)$ will result in a P_{clust} that may fall below the P_{thresh} value that was calibrated for brighter galaxies. As an additional complication, the slope of the blue star-forming galaxy sequence (the blue "cloud") is such that faint blue galaxies are typically bluer than bright blue galaxies, meaning that the photometric redshifts will perform correspondingly worse. To assess whether this effect could cause the downturn on the faint-end LF_{zp} for blue galaxies we examined the dependence of the z_{phot} 68% confidence limits on M_g for blue and red galaxies with $z_{phot} = z_{clust} \pm 0.05$. For red galaxies the internal z_{phot} errors remain small and increase only slowly with M_g. For blue galaxies, however, the internal errors rise more rapidly with increasing M_g and there is a population of blue galaxies with very large errors. Both the blue galaxies with very large errors and those on the upper envelope of the main error–magnitude relation are flagged as interlopers by the photometric redshifts. The absolute magnitude where this increase in the z_{phot} uncertainties of blue galaxies occurs coincides with the magnitude where the faint-end slopes of LF_{ss} and LF_{zp} start diverging. The difficulty in using z_{phot} to establish membership at faint magnitudes is explored further in Pelló et al. (2009). It may be that the best way to study blue galaxies with photometric techniques is by using a combination of statistical background subtraction and photometric redshift membership techniques, such that the photometric redshifts are used as a first-pass membership method and the statistical background subtraction is then used to subtract off any residual (e.g., Kodama et al. 2001; Tanaka et al. 2005). In practice, this will require either a large field sample with identical photometry (and hence photometric redshift performance) as the target field or a cluster image with a wide enough area to have minimal contamination from the cluster at the outskirts of the image.

As mentioned, these two problems in determining the faint end should not be (and apparently are not) as severe for red galaxies as for blue. Photometric redshifts seem to perform better for red galaxies than for blue, at least in the realm of decreasing photometric S/N. The source of the discrepancy between LF_{ss} and LF_{zp} at the bright end is not as clear. The CFDF appears to be slightly underdense with respect to the FORS Deep Field (Heidt et al. 2003) and the COMBO-17 number counts from The CDF-S (Wolf et al. 2004), which would serve to increase the LF_{ss} value for the EDisCS. Also, despite our best efforts at calibration of z_{phot} for bright sources from the spectroscopic sample, the photometric redshifts may reject a slightly larger number of blue members than red members, which would push LF_{zp} down. In the end, we must conclude that the determination of the blue-galaxy cluster LF is not robust when only using photometric redshifts or statistical subtraction.

The red galaxy LFs, however, agree astonishingly well, indicating that the red galaxy LF is robust to the exact method used. We therefore limit most of our subsequent analyses to the red galaxies only.

4.6. The Local Luminosity Function

To measure evolution in the LF it is important to have an appropriate local sample. For many parameters of the galaxy population, e.g., the star-forming fraction (Poggianti et al. 2006) and the early-type fraction (Desai et al. 2007), there is a strong dependence on σ at intermediate- and high redshifts, implying that the evolution can only be measured in samples matched in velocity dispersion. No dependence of the LF of all cluster galaxies on σ has been found at low redshift (De Propris et al. 2003) but we wish to test this for red-sequence galaxies specifically at intermediate- and high redshifts. For our purposes we therefore require a local sample that has the same range in σ as our sample and allows for the computation of an LF just for red-sequence galaxies. It is also desirable that enough local clusters be used so as to average over cluster-to-cluster variations and minimize the uncertainties in the local anchor of any evolutionary trends. Finally, it is advantageous if the local LF has been computed in multiple bands, to allow the measurement of wavelength-dependent evolution. De Propris et al. (2003), Popesso et al. (2005), and Popesso et al. (2006) computed composite, high-S/N LFs from the 2dFGRS and SDSS, respectively. De Propris et al. (2003) compute their LFs only in the b_j band and do not compute them as a function of galaxy color. Popesso et al. (2006) presented composite LFs for X-ray-selected clusters in multiple bands and as a function of galaxy color; however, we choose to construct our own SDSS LF, for the following reasons. The sample of (Popesso et al. 2005; 2006) is X-ray-selected, which may cause biases in the comparison of the local sample to the EDisCS sample, which is optically selected. Second, Popesso et al. (2006) split their LFs by color, but not in an analogous way to the EDisCS sample, which again complicates the comparison to our results. Finally, the raw LFs from (Popesso et al. 2006) are not published, but only the two-component Schechter fits, which also complicates the comparison to our LFs.

Our cluster sample is a subset of the sample presented in von der Linden et al. (2007). This parent sample was selected from the C4 catalog of Miller et al. (2005), but employs improved algorithms to identify the BCG and measure the velocity dispersion. We limit our analysis to clusters at $z \leqslant 0.06$, to ensure that the individual cluster LFs are complete down to the passively evolved limit of the EDisCS clusters (see below), which results in a sample of 167 clusters. With this redshift cut-off we can limit our analysis to galaxies with $r < 20$, where the star/galaxy separation is still robust and where colors can robustly be determined. We use a global field sample drawn from the SDSS DR4 catalog and use the *model* magnitudes to measure

colors and *cmodel* magnitudes to measure the total magnitude. Colors are measured with the *model* magnitude, since that measure adopts the same aperture in different bands. The *cmodel* magnitudes fit a linear combination of an exponential and de Vaucouleurs profile to each galaxy and integrate the combination of these two to derive a total magnitude. It is well known that the Petrosian magnitude of the SDSS misses the flux, especially for early-type galaxies with de Vaucouleurs profiles and *cmodel* magnitudes should be closer to total.

We isolated cluster members using a statistical subtraction technique similar in principle to what was used for the EDisCS clusters, but with some significant modifications. Since photometry of identical depth and bandpass coverage was available for both our local cluster and "field" samples in multiple bands, we performed our statistical subtraction in 4 dimensions, using bins in *r*magnitude as well as bins in $g-r$, $r-i$, and $i-z$, and using 0.5 bins in magnitude and 0.3 mag bins in color. This technique has two main advantages over the 2D, i.e., magnitude and single color, subtraction used in EDisCS. Although interloper galaxies may have identical colors to cluster members in one color, as more colors are considered, it is increasingly difficult to mimic the colors of galaxies at the cluster redshift, thereby increasing the contrast of the cluster against the background and reducing the number of contaminating galaxies. In addition, because we require that retained galaxies have colors matching that of cluster members from g all the way to z, it is possible to robustly determine rest-frame magnitudes for any bands in between, e.g., $g_{\rm rest}$, $r_{\rm rest}$, and $i_{\rm rest}$. Following Pimbblet et al. (2002) here, we also expand the bins in magnitude first and then in color if the number of expected field galaxies exceeds the number of candidate members. We determine rest-frame magnitudes using the *k*-correct software v4.1.4(Blanton et al. 2003). For each cluster we performed 100 Monte Carlo realizations of the subtraction, where each iteration used a new set of random numbers which were then compared against the membership probabilities to determine the cluster membership. The distribution of the LFs for the full Monte Carlo simulation was used to measure the uncertainties in the LF.

To isolate the red sequence in the SDSS clusters we performed an outlier-resistant fit to the CMR of the composite SDSS cluster population using rest-frame magnitudes and colors and only fitting spectroscopically confirmed members with no Hα emission.[21] Evolution corrections to the mean redshift for red galaxies are very small over our redshift range and do not make a difference when fitting the CMR or deriving the LF. Due to the large number of galaxies over a large range in absolute magnitude, we were able to simultaneously fit the slope and zero point of the relation. For measuring the $g_{\rm rest}$ and $r_{\rm rest}$ LFs we fit the CMR in $(g-r)_{\rm rest}$ versus $g_{\rm rest}$ and $(g-r)_{\rm rest}$ versus $r_{\rm rest}$, respectively. For measuring the $i_{\rm rest}$ LF we fit the CMR in $(r-i)_{\rm rest}$ versus $i_{\rm rest}$. Similar as to what was done for the EDisCS sample, we then classified as red galaxies every galaxy within a stripe centered on the CMR in the color and magnitude used above for each rest-frame band. The width of this stripe in each color was chosen to correspond to $\Delta(U-V)_{\rm rest}=0.3$ at $z=0.6$ assuming that the scatter in the CMR is due entirely to age.

We created individual and composite SDSS cluster LFs using identical procedures as with the EDisCS clusters, i.e., binning the individual clusters in absolute magnitude and creating the composite following Colless (1989). For every Monte Carlo realization of the subtraction we computed the Poisson uncertainty on the LF. As with EDisCS, the LFs were computed within $r<0.75$ Mpc and $r<0.5\,R_{200}$ (as computed using Equation (1)). To determine the absolute magnitude limit down to which we construct the LF while probing the same galaxies as in the EDisCS clusters, we took the absolute magnitude limit for our highest redshift EDisCS cluster and corrected it for passive evolution down to $z=0.06$ using a $Z=2.5\,Z_{\odot}$ BC03 SSP model with $z_{\rm form}=2$. For example, the $g_{\rm rest}$-band limit of -18.5 for the highest redshift EDisCS cluster corresponds to a $g_{\rm rest}$-band limit of -17.5 for the SDSS clusters. The $r<20$ apparent magnitude selection is deep enough such that the absolute magnitude limit is the more restrictive cut for all of our SDSS clusters.

We also split our SDSS clusters by σ to match the velocity dispersion bins in the EDisCS sample. We defined the SDSS σ threshold taking into account the redshift evolution in σ that is predicted from the growth of the cluster dark matter halos over time. Using the expected mass accretion history of halos (Bower 1991; Lacey & Cole 1993), Poggianti et al. (2006) used the results of Wechsler et al. (2002) and Bullock et al. (2001) to show that clusters with $\sigma=600$ km s^{-1} at $z=0.6$ will grow into clusters with $\sigma=700$ km s^{-1} by $z=0$ (see Figure 19 of Milvang-Jensen et al. (2008)). We therefore divide our SDSS sample into high and low velocity dispersion bins using $\sigma=700$ km s^{-1} as the divider. There are 159 clusters in the low-σ bin and eight in the high-σ bin. The mean and median uncertainties in the SDSS velocity dispersions is ±62 and ±55 km s^{-1}, respectively.

We fit each Monte Carlo realization of the composite SDSS LF with a Schechter function, allowing all three parameters to vary. The best-fit parameters come from the mean of the realizations and the uncertainties on the parameters come from the 68% confidence intervals of distribution from all Monte Carlo realizations summed in quadrature with the mean formal fit errors. In Figure 3, we show the SDSS LFs for red-sequence galaxies and the corresponding Schechter function fits in each band for the whole cluster sample. The Schechter fit parameters are also given in Table 2.

Table 2
SDSS LF Schechter Function Parameters

Filter	$\sigma_{\rm clust}$	$M_\star$ $M-5\log h_{70}$	α
g	All clusters	$-20.75^{+0.03}_{-0.03}$	$-0.96^{+0.00}_{-0.01}$
g	$\geqslant 700$ km s^{-1}	$-20.54^{+0.04}_{-0.03}$	$-0.92^{+0.03}_{-0.04}$
g	<700 km s^{-1}	$-20.88^{+0.06}_{-0.06}$	$-1.00^{+0.02}_{-0.02}$
r	All clusters	$-21.21^{+0.05}_{-0.04}$	$-0.78^{+0.03}_{-0.02}$
r	$\geqslant 700$ km s^{-1}	$-21.38^{+0.07}_{-0.06}$	$-0.82^{+0.04}_{-0.05}$
r	<700 km s^{-1}	$-21.20^{+0.05}_{-0.05}$	$-0.78^{+0.02}_{-0.03}$
i	All clusters	$-21.46^{+0.03}_{-0.04}$	$-0.75^{+0.02}_{-0.01}$
i	$\geqslant 700$ km s^{-1}	$-21.07^{+0.09}_{-0.10}$	$-0.43^{+0.14}_{-0.13}$
i	<700 km s^{-1}	$-21.53^{+0.04}_{-0.03}$	$-0.78^{+0.02}_{-0.01}$

5. RESULTS

In this section, we present the LFs for red-sequence galaxies in the EDisCS clusters. As we discussed in Section 4.5 we will limit our analysis to the red-sequence LF. Throughout, we will use $\rm LF_{zp}$ since it gives us access to a larger range of rest-frame wavelengths and allows us to go 0.5 mag deeper in our

[21] The presence of Hα was indicated by a measurement of Hα with S/N(Hα)$>$ 5. The Hα measurements were obtained from http://www.mpa-garching.mpg.de/SDSS/DR4/raw_data.html as computed by Brinchmann et al. (2004).

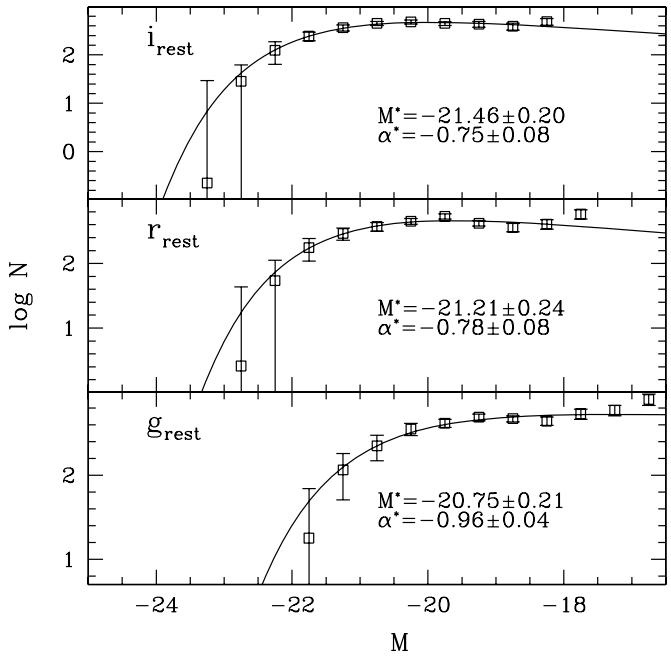

Figure 3. Rest-frame optical composite LFs of red-sequence galaxies for 167 clusters at $z < 0.06$ from the SDSS. The data points, error bars, and solid line represent one of the Monte Carlo iterations of the background subtraction, the Poisson errors, and the corresponding Schechter function fit. The parameters listed are the mean over the full set of Monte Carlo realizations and the error bars on the parameters are the quadrature sum of the Poisson errors and those from our Monte Carlo simulation of the background subtraction errors.

high-redshift clusters (see Section 4.1). We will first present the individual cluster LFs and then the composite LFs split by redshift and velocity dispersion. In all cases, we do not show results for CL1119.3-1129 since this cluster has no NIR data and hence has poorly constrained photometric redshifts. We exclude the CL1103.7-1245a and CL1103.7-1245b clusters at $z = 0.70$ and 0.63 since these clusters overlap on the sky and are too close in redshift to be decomposed with the photometric redshifts. We also exclude CL1103.7-1245 since its redshift ($z = 0.96$) is too high for our imaging to probe far enough down the LF.

5.1. Individual Cluster LFs

In Figure 4, we present the red-sequence LF_{zp} for the remaining 16 EDisCS clusters. The LF of these clusters in the *g*-, *r*-, and *i* bands is given in the Appendix. In all cases, we fix the faint-end slope to the value determined from the composite LF in the relevant redshift range. In general, the Schechter function fits are good with only a few clusters having measured LFs that are of too poor quality to obtain a reasonable fit, e.g., CL1227.9-1138. In most of the remaining cases, it appears that the slope determined from the composite LF is an acceptable fit to the individual clusters, indicating that a universal LF for red-sequence galaxies is possibly in place at these redshifts. There are, however, some exceptions, e.g., CL1301.7-1139 and CL1037.9-1243, where the composite faint-end slope does not seem to adequately represent the cluster LF. There is no significant observed trend of $M^\star$ with cluster redshift. This is in contradiction to the simple expectation that red-sequence galaxies will be brighter in the past due to passive evolution. This will be addressed in the coming sections.

5.2. Composite Cluster LFs

As shown in Figure 4, the S/N of the individual LFs are too low to make any conclusions about trends with redshift or velocity dispersion. For this reason, we create composite clusters splitting the sample into two bins at $z = 0.6$ and in each redshift bin into two bins of velocity dispersion at $\sigma = 600$ km s^{-1}. In all cases, we have used the faint-end slope as determined from the composite in the same redshift bin. The composite LFs are given in Table 3 and the Schechter function parameters for all of the composite LFs are given in Table 4.

5.2.1. Redshift Evolution

In the top panel of Figure 5, we show the composite LFs split by redshift at $z = 0.6$. All LFs are only plotted as faint as they are complete and, for plotting purposes, are all normalized to have the same total integrated luminosity. In the bottom panel, we have corrected the LFs for the passive evolution expected for a population that formed all of its stars at $z = 2$. This formation redshift provides a good fit to the color evolution of the bright red-sequence galaxies in the EDisCS clusters (DL07). At the bright end, we do not have high enough S/N to constrain the detailed evolution precisely. Within the considerable uncertainties, however, it appears that the LFs at the bright end are all similar after applying the correction for passive evolution. This indicates that the bright galaxy population was mostly in place in clusters at $z < 0.8$.

In contrast to the bright end, there is dramatic evolution in the faint-end slope of the LF from $z = 0.8$ to $z = 0$, in the sense that the number of faint galaxies per luminous galaxy increase with decreasing redshift. Other works over recent years have found similar results (DL04; Kodama et al. 2004; Goto et al. 2005; Tanaka et al. 2005; DL07; Stott et al. 2007; Tanaka et al. 2007; Gilbank et al. 2008), although Andreon (2006) finds no such result. Stott et al. (2007) and Gilbank et al. (2008) have large samples of clusters but we measure the LF to 1 mag fainter than that they do at all redshifts. DL04 and DL07 use the same data as in this analysis, but concentrate on the evolution in $N_{\rm lum}/N_{\rm faint}$, as defined using a passively evolving luminosity threshold. Our results using an independent analysis are consistent at the 1σ level with those from DL04 and DL07.

We also fit Schechter functions to the LFs at different redshifts and plot the resulting fits in the top panel of Figure 5. As seen in Table 4 within the EDisCS sample there is strong evolution in α at the 0.5–0.7 level at a significance of 4σ–5σ (depending on the filter). The strong evolution continues down to the SDSS sample with even higher significance. At the same time there is no evidence for evolution in $M^\star$ with redshift. At first glance this seems strange since the bright galaxies are already in place in the clusters and appear to be brighter in the past. However, the evolution in $M^\star$ only tracks the luminosity evolution of the whole galaxy population if all the galaxies evolve in the same way. Given the rapid evolution at the faint end, this is definitely not the case. The highly degenerate nature of α and $M^\star$ make it hard to interpret them simply as an evolution of any given part of the galaxy population. As a side note, the lack of evolution in $M^\star$ that we observe is also consistent at the 1σ–2σ level with the results of Tanaka et al. (2005), who also find a strongly evolving faint end.

Stronger constraints on the joint evolution of the Schechter function parameters would be enabled most effectively by higher S/N at the bright end, as our sample at fainter magnitudes is statistically quite robust. The small number of bright galaxies

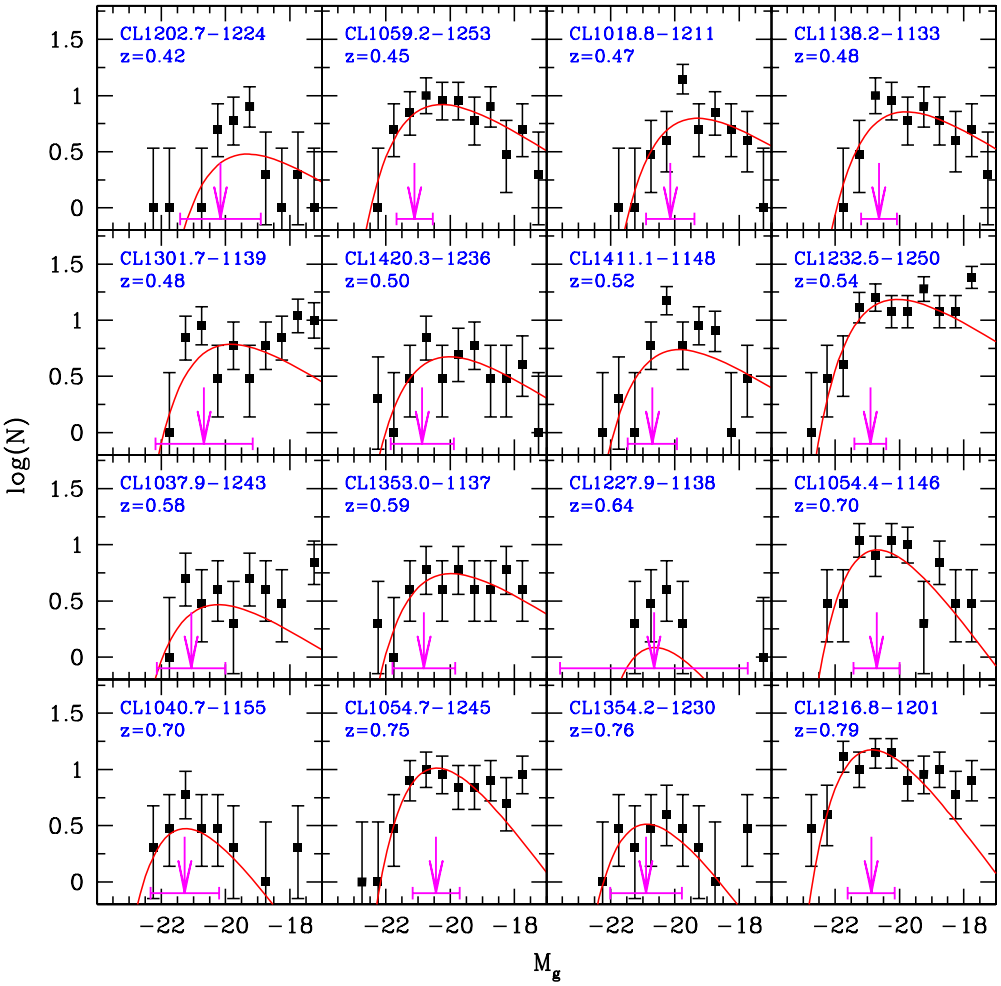

Figure 4. $g_{\rm rest}$-band LFs of red-sequence galaxies in the 16 EDisCS clusters for which $\rm LF_{zp}$ could be determined. The clusters increase in redshift to the right and down. The solid curve gives the best-fit Schechter function with a slope fixed to the values fit to the EDisCS composite LF in the corresponding redshift bin. The arrow and the associated error bar indicate the fitted value of $M^\star$and its 68% confidence limits, respectively.

(A color version of this figure is available in the online journal.)

is a direct consequence of our limited number of clusters and of their modest mass (or richness). The best way to improve the constraints on the Schechter function parameters will be to construct LFs for much larger samples of clusters.

In Section 6.1, we will discuss this further and present implications for the formation histories of red-sequence galaxies in clusters.

5.2.2. Sample Split by Velocity Dispersion

We also examined the differences between the red-sequence LFs when we split our sample by cluster velocity dispersion at $\sigma = 600$ km s^{-1}. The SDSS sample was split at $\sigma = 700$ km s^{-1} corresponding to the expected growth of clusters over time (see Section 4.6.) To assess the differences we take the ratio of the LFs in different σ bins and show the ratio in Figure 6. In this figure trends of the ratio with magnitude illustrate differences between the high- and low-velocity dispersion clusters. There are no major trends with magnitude but in the $0.42 < z < 0.6$ redshift bin the low-velocity dispersion clusters have systematically more faint galaxies relative to bright galaxies, than high-velocity dispersion clusters. Still, formally all these relations are statistically consistent with a constant. As part of their analysis of $N_{\rm lum}/N_{\rm faint}$, DL07 and Gilbank et al. (2008) also divided their samples by velocity dispersion and cluster richness, respectively. For reference, we draw vertical lines in the bottom panel of Figure 6 that correspond to the dividing lines between luminous and faint galaxies from DL07. Calculating $N_{\rm lum}/N_{\rm faint}$ as in DL07 we find entirely consistent results for the EDisCS sample and plot them in Figure 7. For SDSS clusters we find no significant difference between the LFs for clusters of different velocity dispersions, whereas DL07 found a small difference.[22] Our SDSS cluster sample is about twice as large as that of DL07, uses a more sophisticated method for the background subtraction, and uses model magnitudes instead of Petrosian magnitudes. Because of the improvements to our SDSS LF with respect that in DL07 we believe our result although the conclusions are in any case not sensitive to the difference. In addition, the lack of a dependence of $N_{\rm lum}/N_{\rm faint}$ on σ for local clusters agrees with the results from De Propris et al. (2003) who found that their b_J LFs were consistent at the 2σ level for clusters with σ greater and less than 800 km s^{-1}. It must be noted, however, that we only consider the red-sequence cluster LF and therefore it is not possible to directly compare with the results of De Propris et al. (2003). Taken together, our results imply that the higher velocity dispersion

[22] DL07 split their SDSS sample at 600 km s^{-1} but found no difference when splitting at 700 km s^{-1}, although they only had four clusters in their $\sigma >$ 700 km s^{-1} bin.

Table 3
EDisCS Composite LFs

M	$0.4 < z < 0.8$ All Clusters Φ	$0.4 < z < 0.6$ All Clusters Φ	$0.4 < z < 0.6$ >600 (km s^{-1}) Φ	$0.4 < z < 0.6$ <600 (km s^{-1}) Φ	$0.6 < z < 0.8$ All Clusters Φ	$0.6 < z < 0.8$ >600 (km s^{-1}) Φ	$0.6 < z < 0.8$ <600 (km s^{-1}) Φ
			g Band				
$-24.5 < M_g < -24.0$	<7.03	<4.05	<2.83	<2.52	<5.37	<2.99	<3.46
$-24.0 < M_g < -23.5$	<7.03	<4.05	<2.83	<2.52	<5.37	<2.99	<3.46
$-23.5 < M_g < -23.0$	<7.03	<4.05	<2.83	<2.52	<5.37	<2.99	<3.46
$-23.0 < M_g < -22.5$	2.69 ± 7.19	0.38 ± 4.08	0.48 ± 2.89	<2.52	2.12 ± 5.54	1.84 ± 3.26	0.50 ± 3.51
$-22.5 < M_g < -22.0$	22.23 ± 9.94	10.32 ± 6.04	6.05 ± 4.48	4.11 ± 3.65	11.35 ± 7.42	8.19 ± 5.27	3.56 ± 4.41
$-22.0 < M_g < -21.5$	42.49 ± 11.70	17.71 ± 7.01	8.77 ± 4.93	8.01 ± 4.34	23.46 ± 8.79	19.22 ± 7.25	6.08 ± 4.82
$-21.5 < M_g < -21.0$	92.96 ± 16.40	46.53 ± 9.82	28.96 ± 7.32	17.51 ± 5.91	44.55 ± 12.33	22.58 ± 7.12	19.26 ± 7.87
$-21.0 < M_g < -20.5$	118.55 ± 17.77	72.31 ± 11.43	50.47 ± 9.45	23.94 ± 6.42	45.52 ± 12.86	24.81 ± 7.68	18.72 ± 8.13
$-20.5 < M_g < -20.0$	127.00 ± 18.88	71.93 ± 11.61	48.00 ± 9.24	25.14 ± 6.70	53.58 ± 14.01	30.55 ± 8.49	21.29 ± 8.82
$-20.0 < M_g < -19.5$	114.53 ± 17.10	79.37 ± 12.13	39.01 ± 8.61	36.09 ± 7.48	35.69 ± 11.54	23.12 ± 7.66	12.65 ± 7.06
$-19.5 < M_g < -19.0$	90.43 ± 14.04	77.84 ± 12.23	42.72 ± 8.59	32.73 ± 7.58	14.98 ± 7.20	13.02 ± 6.28	3.47 ± 3.77
$-19.0 < M_g < -18.5$	81.18 ± 13.30	62.33 ± 10.94	38.80 ± 8.47	23.46 ± 6.44	20.01 ± 7.57	15.85 ± 5.94	5.49 ± 4.28
$-18.5 < M_g < -18.0$	56.21 ± 11.72	49.15 ± 10.17	31.17 ± 7.81	18.16 ± 6.01	8.65 ± 6.05	6.66 ± 4.04	2.48 ± 3.69
$-18.0 < M_g < -17.5$	76.73 ± 13.09	54.11 ± 9.60	44.58 ± 8.53	13.84 ± 5.06	23.09 ± 8.57	16.16 ± 7.10	7.52 ± 4.68
			r Band				
$-24.5 < M_r < -24.0$	<6.60	<4.00	<2.94	<2.45	<4.94	<3.06	<3.02
$-24.0 < M_r < -23.5$	0.53 ± 6.64	<4.00	<2.94	<2.45	0.48 ± 4.98	0.63 ± 3.16	<3.02
$-23.5 < M_r < -23.0$	5.19 ± 7.12	2.70 ± 4.57	2.28 ± 3.78	0.66 ± 2.59	2.44 ± 5.19	2.20 ± 3.47	0.52 ± 3.09
$-23.0 < M_r < -22.5$	29.88 ± 10.40	12.48 ± 6.26	7.59 ± 4.85	4.85 ± 3.72	16.49 ± 7.82	9.76 ± 5.42	6.25 ± 4.60
$-22.5 < M_r < -22.0$	57.23 ± 13.33	21.98 ± 7.59	8.03 ± 4.82	11.83 ± 4.97	33.23 ± 10.24	26.48 ± 8.38	8.99 ± 5.53
$-22.0 < M_r < -21.5$	101.63 ± 15.94	60.24 ± 10.61	41.29 ± 8.93	20.51 ± 5.93	40.30 ± 11.25	20.49 ± 7.03	17.07 ± 6.85
$-21.5 < M_r < -21.0$	109.67 ± 16.65	64.73 ± 10.85	47.36 ± 9.09	20.18 ± 6.09	43.92 ± 11.93	27.43 ± 8.44	15.90 ± 6.96
$-21.0 < M_r < -20.5$	118.39 ± 17.46	71.33 ± 11.50	44.50 ± 9.25	26.99 ± 6.67	48.12 ± 12.62	24.58 ± 7.26	20.33 ± 7.86
$-20.5 < M_r < -20.0$	101.41 ± 15.16	79.59 ± 12.29	38.57 ± 8.79	36.96 ± 7.66	24.60 ± 9.03	17.66 ± 6.85	7.69 ± 5.10
$-20.0 < M_r < -19.5$	83.02 ± 13.36	70.37 ± 11.54	43.40 ± 8.84	26.93 ± 6.92	16.33 ± 7.32	15.44 ± 7.17	3.13 ± 3.36
$-19.5 < M_r < -19.0$	71.75 ± 12.58	60.04 ± 10.72	33.40 ± 8.13	25.23 ± 6.47	14.26 ± 6.93	11.03 ± 5.59	4.04 ± 3.78
$-19.0 < M_r < -18.5$	50.30 ± 10.80	43.58 ± 9.34	30.64 ± 7.60	14.35 ± 5.37	7.83 ± 5.65	6.30 ± 4.08	2.08 ± 3.26
$-18.5 < M_r < -18.0$	...	54.94 ± 10.16	37.95 ± 8.13	18.51 ± 5.92	...	...	...
$-18.0 < M_r < -17.5$	...	...	...	...	...	...	...
			i Band				
$-24.5 < M_i < -24.0$	<6.45	<3.90	<2.77	<2.51	<4.84	<3.00	<3.12
$-24.0 < M_i < -23.5$	1.93 ± 6.55	0.41 ± 3.94	0.50 ± 2.85	<2.51	1.42 ± 4.94	1.86 ± 3.27	<3.12
$-23.5 < M_i < -23.0$	22.48 ± 9.41	10.20 ± 5.87	6.02 ± 4.41	4.14 ± 3.65	11.82 ± 6.97	8.18 ± 5.27	3.89 ± 4.09
$-23.0 < M_i < -22.5$	40.15 ± 10.90	17.43 ± 6.89	8.15 ± 4.80	8.49 ± 4.47	21.73 ± 8.01	17.50 ± 6.63	5.84 ± 4.45
$-22.5 < M_i < -22.0$	87.44 ± 15.39	42.04 ± 9.32	23.16 ± 6.73	18.15 ± 5.93	42.87 ± 11.48	23.65 ± 7.69	17.65 ± 7.16
$-22.0 < M_i < -21.5$	108.61 ± 16.03	64.97 ± 10.42	54.26 ± 9.53	15.84 ± 5.39	41.78 ± 11.44	23.35 ± 7.12	17.12 ± 7.36
$-21.5 < M_i < -21.0$	119.74 ± 17.39	67.00 ± 10.95	43.61 ± 8.72	24.50 ± 6.54	52.02 ± 12.84	31.93 ± 8.93	19.85 ± 7.98
$-21.0 < M_i < -20.5$	97.43 ± 15.34	68.10 ± 11.41	31.05 ± 7.82	33.68 ± 7.46	29.81 ± 9.92	17.13 ± 6.08	11.93 ± 6.41
$-20.5 < M_i < -20.0$	88.31 ± 13.66	72.39 ± 11.42	39.31 ± 8.33	31.64 ± 7.23	17.87 ± 7.56	17.38 ± 7.66	3.10 ± 3.45
$-20.0 < M_i < -19.5$	78.96 ± 12.73	68.22 ± 11.14	39.00 ± 8.16	28.52 ± 7.03	12.40 ± 6.29	8.59 ± 4.32	4.01 ± 3.86
$-19.5 < M_i < -19.0$	51.95 ± 11.05	42.79 ± 9.16	26.64 ± 7.08	16.45 ± 5.59	10.27 ± 6.18	8.44 ± 5.24	2.59 ± 3.40
$-19.0 < M_i < -18.5$	...	51.44 ± 10.03	32.30 ± 7.75	19.60 ± 6.12	...	...	4.01 ± 3.86
$-18.5 < M_i < -18.0$	...	...	...	...	...	...	...
$-18.0 < M_i < -17.5$	...	...	...	...	...	...	...

Notes. Magnitudes are given in units of $M - 5\log h_{70}$. Composite LFs are only given for magnitudes brighter than which all clusters in each redshift and velocity bin are complete.

clusters evolved at a faster rate than the low-velocity dispersion clusters. A dependence on cluster velocity dispersion is also seen by Poggianti et al. (2006) who find that the fraction of star-forming members in clusters evolves most quickly in clusters with velocity dispersions similar to those for the most massive 50% of the EDisCS clusters.

Gilbank et al. (2008) analyzed the dependence of $N_{\rm lum}/N_{\rm faint}$ on cluster richness and also found that richer clusters evolve quicker than clusters with low richness. They also find that low-richness clusters at $0.4 < z < 0.6$ have a higher $N_{\rm lum}/N_{\rm faint}$ than high-richness clusters. This is in the opposite sense of the trend found by DL07 and our work, in that higher velocity dispersion clusters have a higher $N_{\rm lum}/N_{\rm faint}$ than low-velocity dispersion clusters. While this difference in our work is not very significant, the difference between our results and those of Gilbank et al. (2008) seems to be as they go in opposite directions. Unfortunately it is difficult to make a straightforward comparison between our results as Gilbank et al. (2008) split their clusters at a richness that corresponds to $\sim$ 400 km s^{-1}, below which we only have four clusters. We therefore have almost no constraint on the behavior of $N_{\rm lum}/N_{\rm faint}$ for these very poor systems. To resolve this discrepancy will require computing $N_{\rm lum}/N_{\rm faint}$ in the Gilbank sample with our velocity dispersion cut. Another difference in Gilbank et al. (2008)

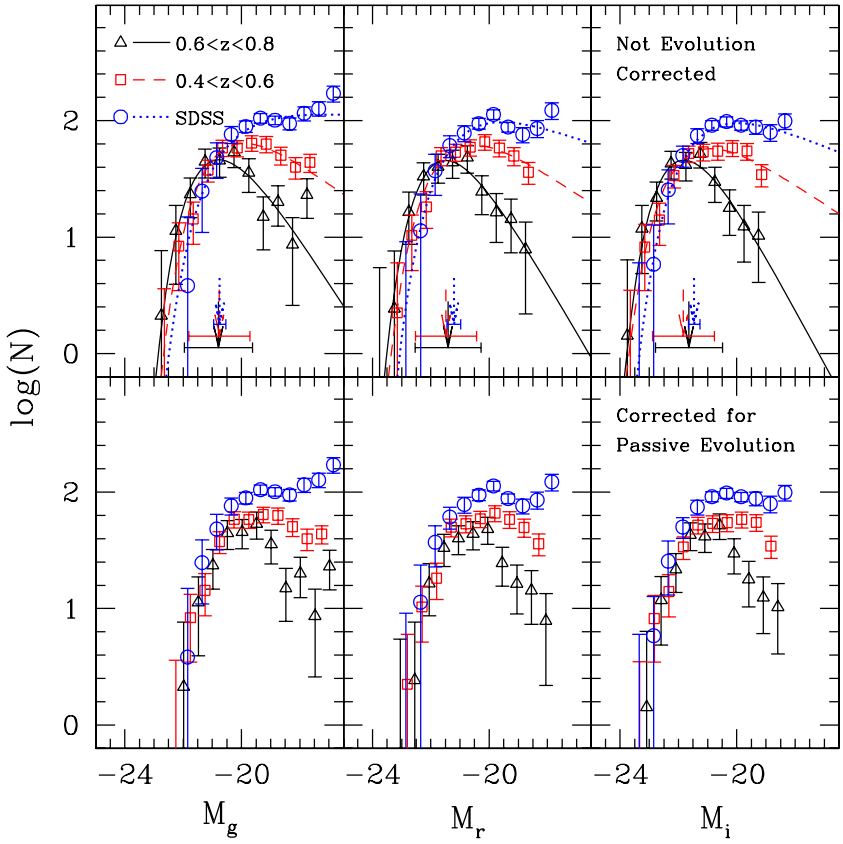

Figure 5. Composite rest-frame *g*-, *r*-, and *i* LFs of red-sequence EDisCS and SDSS cluster galaxies split into bins of redshift. The composites at $0.6 < z < 0.8$ and $0.4 < z < 0.6$ have six and 10 clusters, respectively. All plotted LFs and their fits have been scaled so that the total luminosity density of the best fits is equal. Top row: the LFs are presented without any evolution correction. Vertical arrows and horizontal error bars give the value of $M^\star$ and the 68% confidence interval. The top, middle, and bottom arrows correspond to the SDSS, intermediate-redshift EDisCS clusters, and high-redshift EDisCS clusters, respectively. The points for the two EDisCS LFs have been offset slightly in magnitude for plotting clarity. Bottom row: the LFs have all been corrected for passive evolution to the mean redshift of the SDSS clusters. All symbols are as in the top panel. The luminous red-sequence galaxies are all in place out to $z = 0.8$ but the fainter red-sequence galaxies built up dramatically over time.

(A color version of this figure is available in the online journal.)

Table 4
Schechter Function Parameters for EDisCS Composite LFs

Redshift	$\sigma_{\rm clust}$	$M_g^\star$ $M - 5\log h_{70}$	α_g	$M_r^\star$ $M - 5\log h_{70}$	α_r	$M_i^\star$ $M - 5\log h_{70}$	α_i
$0.4 < z < 0.8$	all clusters	$-20.92^{+0.21}_{-0.15}$	$-0.45^{+0.13}_{-0.08}$	$-21.51^{+0.23}_{-0.14}$	$-0.36^{+0.16}_{-0.08}$	$-21.80^{+0.22}_{-0.17}$	$-0.34^{+0.16}_{-0.10}$
$0.4 < z < 0.6$	all clusters	$-20.76^{+0.24}_{-0.16}$	$-0.54^{+0.13}_{-0.08}$	$-21.48^{+0.26}_{-0.14}$	$-0.58^{+0.13}_{-0.06}$	$-21.83^{+0.28}_{-0.14}$	$-0.58^{+0.15}_{-0.06}$
$0.4 < z < 0.6$	$\geqslant 600$ km s^{-1}	$-20.73^{+0.14}_{-0.10}$	...[b]	$-21.38^{+0.12}_{-0.10}$	...[b]	$-21.81^{+0.12}_{-0.12}$	...[b]
$0.4 < z < 0.6$	< 600 km s^{-1}	$-20.80^{+0.20}_{-0.14}$	...[b]	$-21.50^{+0.20}_{-0.14}$	...[b]	$-21.75^{+0.22}_{-0.16}$	...[b]
$0.6 < z < 0.8$	all clusters	$-20.79^{+0.40}_{-0.26}$	$-0.02^{+0.41}_{-0.18}$	$-21.41^{+0.38}_{-0.20}$	$0.08^{+0.41}_{-0.15}$	$-21.64^{+0.38}_{-0.24}$	$0.17^{+0.42}_{-0.20}$
$0.6 < z < 0.8$	$\geqslant 600$ km s^{-1}	$-20.77^{+0.18}_{-0.14}$	...[a]	$-21.37^{+0.18}_{-0.14}$	...[a]	$-21.67^{+0.18}_{-0.14}$	...[a]
$0.6 < z < 0.8$	< 600 km s^{-1}	$-20.81^{+0.26}_{-0.22}$	...[a]	$-21.46^{+0.22}_{-0.20}$	...[a]	$-21.66^{+0.22}_{-0.18}$	...[a]

Notes.
[a] Uses distribution of α determined from fits to all clusters at $0.6 < z < 0.8$.
[b] Uses distribution of α determined from fits to all clusters at $0.4 < z < 0.6$.

with respect to our work is that those authors use a color cut that isolates only the red side of the red sequence, whereas our color cut encompasses a band centered on the peak of the red sequence. It is possible, therefore, that our cut has a different contribution from blue galaxies at the blue side of the red sequence. It is not clear, however, which cut is more physically meaningful. While the Gilbank et al. (2008) cut only isolates galaxies with the reddest colors it may miss galaxies that have been most recently added to the red sequence and therefore those that have the youngest stellar population ages and bluest colors. At present we cannot determine the nature of the discrepancy as a cut only on the red side of the red sequence in our data would substantially reduce the significance which we can measure $N_{\rm lum}/N_{\rm faint}$.

We do not have enough galaxies to reliably fit α and $M^\star$ independently for our composite LFs split by velocity dispersion. Because these two parameters are highly degenerate and there are indications that $N_{\rm lum}/N_{\rm faint}$ is different in the different bins of σ we therefore do not attempt to interpret the Schechter function fits split by σ.

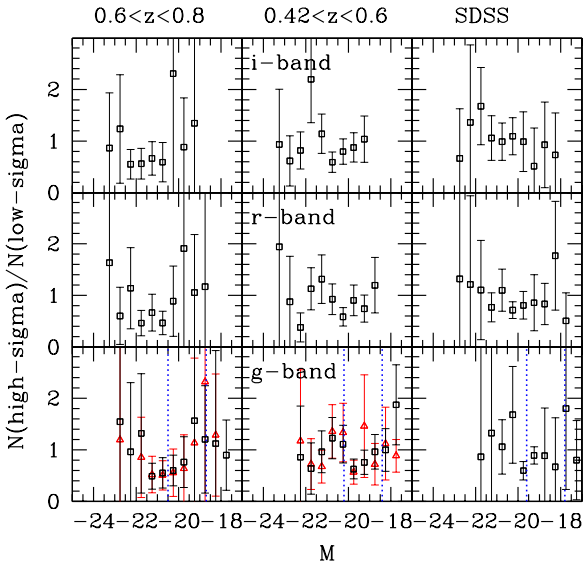

Figure 6. Ratio of the LF of red-sequence galaxies in clusters of different velocity dispersions. Large differences in the shapes of the LFs will appear as significant deviations from a horizontal line in this plot. Each column indicates a different redshift bin and each row represents a different rest-frame band. The ratio has been normalized to a mean of unity to demonstrate relative differences with magnitude. For the *g*-band LF for EDisCS clusters we show the ratio of LF_{ss} as red triangles to compare the ratio of LF_{zp} given as black squares. All EDisCS points for the *r* and *i* bands are using LF_{zp}. The vertical dotted lines in the bottom row give the division between bright and faint galaxies that correspond to those used in De Lucia et al. (2007).

(A color version of this figure is available in the online journal.)

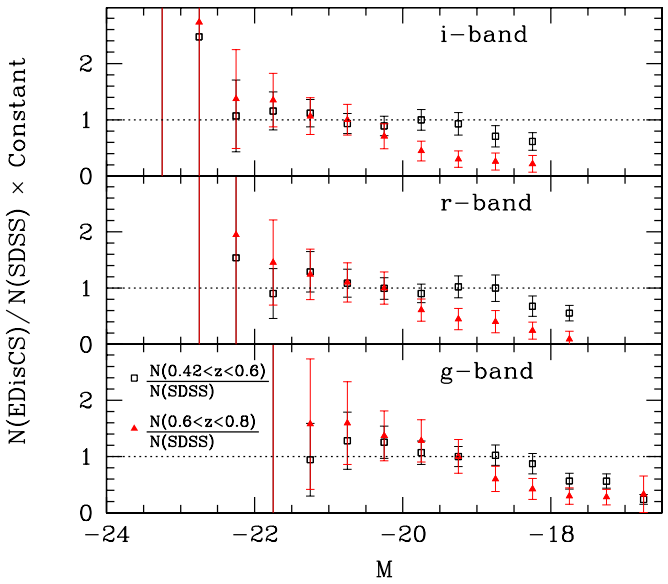

Figure 8. Ratio of the EDisCS composite red-sequence LFs to those from the SDSS in the rest-frame *g*, *r*, and *i* bands. In all cases, the EDisCS LFs have been corrected for passive evolution expected for a population that formed its stars at $z = 2$. The ratio has also been scaled to have a median of unity to allow comparisons of the intermediate- and high-redshift EDisCS clusters. The horizontal lines are drawn at unity to guide the eye. In all three bands, the bright end is consistent with a constant value, which appears to turn over at fainter magnitudes. The turnover magnitude evolves to fainter magnitudes at lower redshifts.

(A color version of this figure is available in the online journal.)

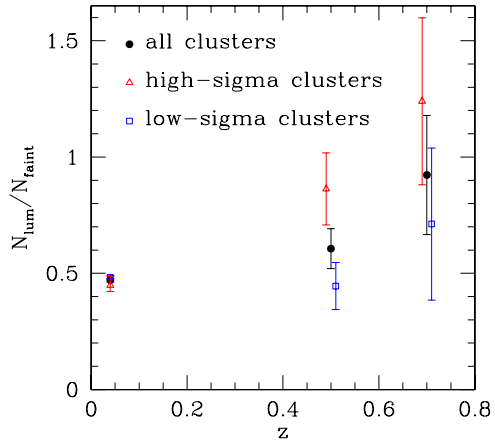

Figure 7. Ratio of luminous-to-faint red-sequence galaxies in clusters at $z < 0.8$. The dividing line between luminous and faint galaxies has been corrected for passive evolution and is similar to that used in De Lucia et al. (2007). There is a trend that the high-velocity dispersion clusters evolve quicker than the lower velocity dispersion clusters and there is no difference with velocity dispersion in the SDSS clusters.

(A color version of this figure is available in the online journal.)

5.2.3. Radial Gradients

We examined whether there was any evidence for radial gradients in the LF. We do not have enough galaxies to split our clusters up into annuli so instead we compared the LFs within 0.75 and 0.5 Mpc, with the acknowledgment that these two are correlated. For both the clusters at $0.4 < z < 0.6$ and those at $0.6 < z < 0.8$ the galaxies at 0.5 Mpc $< r <$ 0.75 Mpc make up $\sim 30\%$ of the galaxies at $r < 0.75$ Mpc. For the EDisCS clusters we made a similar comparison as in Figure 6 and find that there are no significant differences in the LFs at different radii. As expected from this, there are also no significant differences in the Schechter function parameters. These results are true for all rest-frame filters. In their study of local clusters, Paolillo et al. (2001) find results consistent with ours but for the whole galaxy population instead of just for those on the red sequence. Popesso et al. (2006) measure the red-sequence LF at different radii in local clusters and find that there are radial trends in the LF, but primarily at magnitudes fainter than what we probe with our data. At magnitudes corresponding to those we probe they find only a weak dependence of the LF with cluster radius, which is entirely compatible with our lower precision measurement of the radial trends. Hansen et al. (2007) measure the LF of red galaxies in different radial bins in many more clusters than Popesso et al. (2006) but to significantly brighter magnitude limits and also find no radial dependence in the shape of the LF.

6. DISCUSSION

6.1. Mass-Dependent Build-up of Red-Sequence Cluster Galaxies

As shown in Section 5.2.1 and Figure 5, there is dramatic evolution in the LFs of red-sequence galaxies from $z = 0.8$ to $z = 0$. At the same time this evolution appears to proceed at different rates for galaxies of different luminosities. Red sequence galaxies at $L \gtrsim L^{\star}$ appear to be in place at $z \sim 0.8$ but the fainter galaxies were added to the red sequence at much later times. As a different way to visualize this we plot in Figure 8 the ratio of the passive-evolution-corrected EDisCS LFs to those from the SDSS. At bright magnitudes both LFs are consistent with a constant ratio, implying that the EDisCS and SDSS LFs have the same shape. At fainter magnitudes the ratio then decreases. In the intermediate-redshift clusters

it appears that there is a threshold magnitude, fainter than which there is a deficit of red-sequence galaxies with respect to the SDSS clusters and above which there appears to be a constant ratio. For the high-redshift clusters there is not enough S/N to determine if a threshold magnitude exists or if there is simply a monotonic trend to fainter magnitudes. In any case, it is clear that the magnitude brighter than which the red sequence is in place is fainter at lower redshifts. This is reminiscent of the results by Bundy et al. (2006) who show that there is a threshold stellar mass above which star formation appears to be quenched in field galaxies, and that this threshold evolves to lower masses at lower redshifts. However, cluster-associated processes for quenching star formation, e.g., ram-pressure stripping, strangulation/starvation, or harassment, are different from the mass-dependent quenching that may be present in the field. It may be that the evolving mass threshold in the field is imprinted on the cluster red sequence in the form of infalling red galaxies whose star formation is halted for reasons not associated with the cluster. We cannot, however, directly confirm that hypothesis with our data. It will be very interesting in the future to compare the mass functions of cluster and field galaxies to see if there are differences between the cluster and the field.

These results imply that the bright cluster galaxies were already in place and on the red sequence by $z = 0.8$. This is consistent with the evolution of the colors of these galaxies, which is fitted well by an SSP with $2 < z_{\rm form} < 3$ (Stanford et al. 1998; Holden et al. 2004; DL07). It is also perfectly consistent with the formation redshifts found by fundamental plane studies (e.g., van Dokkum & Franx 2001; van der Wel et al. 2005; Jørgensen et al. 2006; van Dokkum & van der Marel 2007; R. Saglia et al. 2009, in preparation). Barger et al. (1998) found no formal evidence of evolution in their K-band LF for morphologically classified early-type galaxies, but had large enough error bars to be compatible with the expected amount of passive evolution over their redshift interval. They did perform an analysis of the surface brightness evolution, however, and found the amount of fading expected from passive evolution. Later works performed more extensive LF analyses using K-band LF (De Propris et al. 1999), and in the rest-frame NIR (Andreon 2006; De Propris et al. 2007) and find evolution in $M^\star$ consistent with passive evolution and $z_{\rm form} > 1.5$ when fit to galaxies with a faint limit 1–3 mag brighter than ours. This may imply that the red-sequence galaxies dominate the galaxy mass function of clusters even out to $z \sim 0.8$, such that the total LF of bright galaxies in the rest-frame NIR is really dominated by red-sequence galaxies. We will address this directly in our future analysis of the galaxy stellar mass function in our clusters (A. Aragón-Salamanca et al. 2009, in preparation).

In previous works, the high inferred formation redshift for bright red galaxies has been used by many LF studies to imply that the population of all red-sequence cluster galaxies was already in place at $z > 1$. We, however, have shown that there is indeed a differential build-up of the red sequence with redshift, such that fainter galaxies were added to the red sequence at lower redshifts than brighter galaxies. This may in fact be consistent with claims that the early-type fraction increased significantly at $z < 1$ (e.g., Dressler et al. 1997; Fasano et al. 2000; Smith et al. 2005; Postman et al. 2005; Desai et al. 2007) implying a late buildup of significant fractions of the red galaxy population. This is explored in more detail in Sanchez-Blazquez et al. (2009), which examines the joint evolution of ages, metallicities, and morphologies of galaxies on the red sequence.

6.2. Comparison to Field

We compare our red-sequence LF to two independently computed red-sequence LFs for the field.[23] The first field LF is that published by Brown et al. (2007) in the NDWFS. The NDWFS LF is computed over 6.96 deg^2. It is somewhat shallower than the EDisCS survey but the LF has excellent S/N at both the bright and faint end of the LF. Magnitudes in the NDWFS were measured in circular apertures of $r = 4\farcs0$ and had an aperture correction derived from simulations. Although our surveys have substantially different depth and image quality, we have checked that our total magnitude estimates are compatible with those in the NDWFS. We compared the aperture corrections we apply to our AUTO magnitudes in EDisCS with the difference between the AUTO magnitudes of NDWFS galaxies and their total magnitude estimate (Brown et al. 2007). This difference is similar, indicating that our correction brings our total magnitudes into rough agreement with theirs. Both our survey and the NDWFS select red galaxies in similar ways, implying that our results can directly be compared.

For our second comparison we determine the LF for red-sequence galaxies using a modified version of the data and the LF technique presented in Marchesini et al. (2007). The original data are comprised of multiband optical through NIR photometry over six dispersed fields, with a total area of 355 arcmin^2. The fields are comprised of the Hubble Deep Field South, The Chandra Deep Field South, and the four fields from the Deep NIR Multi-Wavelength Survey by Yale-Chile (MUSYC; Quadri et al. 2007). The main modification that we have made to the data presented in Marchesini et al. (2007) is that we have included photometry past the K band to 8.0 μm using *Spitzer* observations (Wuyts et al. 2008; Marchesini et al. 2009). We have also determined the photometric redshifts using a different code (EAZY; Brammer et al. 2008). The data are K-selected but we used the observed $I-K$ colors of galaxies at $z < 1$ in the EDisCS I-band-selected catalog to verify that we can detect all red-sequence galaxies in the K-band data at $z < 1$. Therefore, we can use the K-band selected data to construct a pseudo-I-band-selected red-sequence sample analogous to that for EDisCS. Total magnitudes in the MUSYC survey are constructed using SExtractor AUTO apertures with aperture corrections derived in an identical way as our own. The MUSYC red-sequence definition is identical to our own and that from Brown et al. (2007) is very similar, ensuring that we are selecting red-sequence galaxies in the same way.

The NDWFS red galaxy LFs are consistent with those from COMBO-17 (Bell et al. 2004) and DEEP2 (Willmer et al. 2006; Faber et al. 2007) but are derived over a much larger area and have a very well determined bright end. The NDWFS LF is only computed in the rest-frame B band and so we compare it to the EDisCS LF also computed in the rest-frame B band. The MUSYC LFs are statistically consistent with the NDWFS LFs at bright magnitudes but go significantly deeper and have LFs in the g-, r-, and i bands. In both field samples, the Schechter function fits to the field data have been performed using a maximum-likelihood technique with α as a free parameter and the plotted points are the $1/V_{\rm max}$ measurements of the LF

[23] There are other measures of the early-type galaxy LF in the field at $z = 1$ (e.g., Zucca et al. 2006; Scarlata et al. 2007) but we choose not to compare directly with these surveys for various reasons. For example, Zucca et al. (2006) identify red galaxies by spectroscopic type and it is not clear how that corresponds to our selection by color. Scarlata et al. (2007) do not aperture correct their magnitude measures and their LFs are 1–2 mag shallower than ours, while not having a higher S/N than the NDWFS.

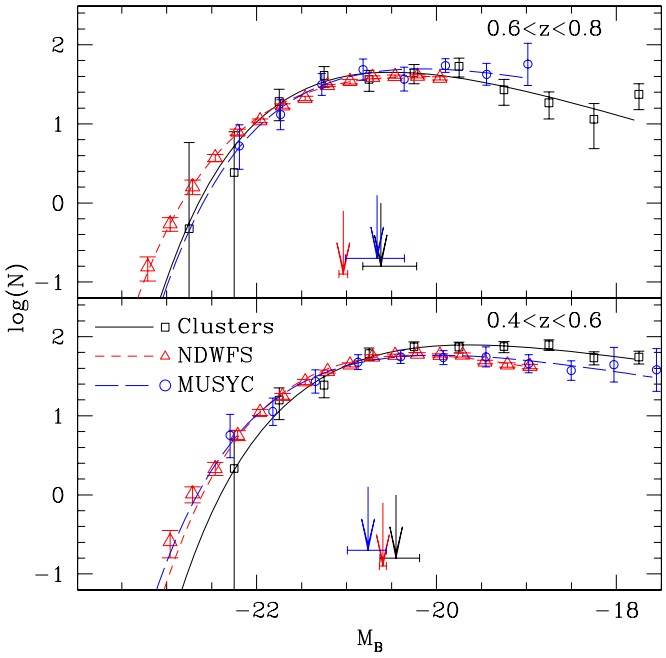

Figure 9. Comparison of the *B*-band LFs and Schechter function fits for the composite LF of red-sequence galaxies in EDisCS clusters and the LF of red-sequence galaxies in the field as determined from the NDWFS (Brown et al. 2007) and from MUSYC, in two redshift bins. The vertical arrows give the values of $M^\star$ and its 68% confidence limits. The upper, middle, and lower arrows refer to the MUSYC, EDisCS, and NDWFS LFs, respectively. We have used the NDWFS Schechter fits that allow α to vary. The field LFs have been scaled vertically to have the same total luminosity density as the EDisCS LF.

(A color version of this figure is available in the online journal.)

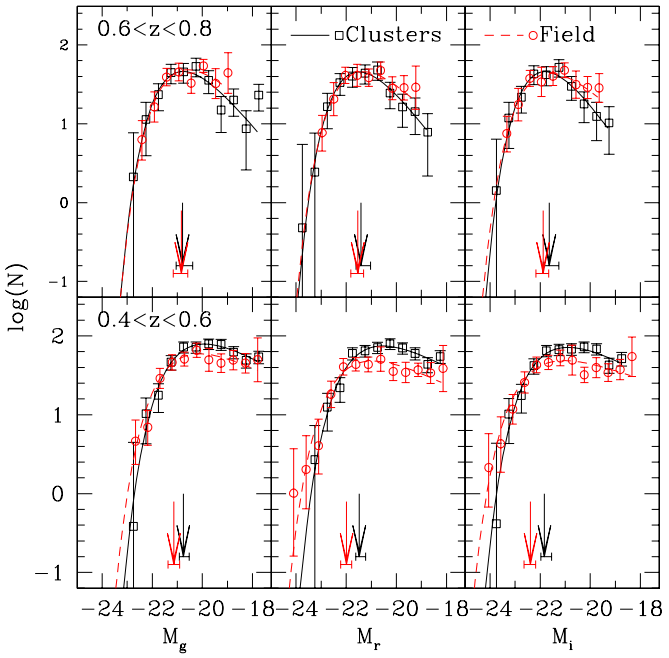

Figure 10. Comparison of the *g*, *r*, and *i* band LFs and Schechter function fits for the composite LF of red-sequence galaxies in EDisCS clusters and the LF of red-sequence galaxies in the field (as determined from the MUSYC survey), in two redshift bins. The vertical arrows give the values of $M^\star$ and its 68% confidence limits. The upper and lower arrows refer to the EDisCS and MUSYC survey, respectively. The field LF has been scaled vertically to have the same total luminosity density as the EDisCS LF.

(A color version of this figure is available in the online journal.)

which include the contribution from field-to-field variance for the MUSYC data.

We compare the field LFs to those from EDisCS in Figures 9 and 10. In both figures for display purposes we have normalized the different LFs to have the same integrated luminosity. The bright ends of the field and clusters are consistent in all cases. At fainter magnitudes, the cluster LF appears to be overabundant compared to the field at $0.4 < z < 0.6$, but this trend reverses itself at $0.6 < z < 0.8$. The reversal is most apparent at the reddest rest-frame wavelengths (the right two columns of Figure 10), where the MUSYC LF extends to similar depths as the EDisCS LF.

With regards to the best-fit Schechter function parameters, those from the two-field surveys agree with each other at better than 1.5σ. It appears that the field value of $M^\star$ is systematically brighter than for the clusters in both redshift bins, but only at the $\sim 2\sigma$ level. At $0.4 < z < 0.6$ the faint-end slope of the clusters is steeper than for the field at the $\sim 2\sigma$ level. At $0.6 < z < 0.8$ however, this has reversed, with the field having an α that is $\sim 2\sigma$ steeper than for clusters. The change in the relative slopes is interesting as, in addition to the dependence of $N_{\rm lum}/N_{\rm faint}$ evolution on cluster velocity dispersion presented in Section 5.2.2, it provides further indication that the buildup of the red sequence happens at different rates in different environments. Further it appears that the population of the faint end of the red sequence happens more quickly in clusters than in the field. This could occur if the main channels for the population of the red sequence in the field occur at a roughly constant or decreasing rate with increasing cosmic time, as may be the case for AGN feedback (e.g., Croton et al. 2006) or galaxy–galaxy mergers (e.g., Lotz et al. 2008), while quenching processes associated with clusters become more efficient with increasing time. This is plausible in a ΛCDM universe where cluster assembly proceeds most rapidly at late times, implying that the processes associated with quenching in clusters would also become more efficient as one moves toward lower redshift. At face value, this is consistent with the results of Desai et al. (2007), who found that the S0 fraction in clusters from EDisCS and Fasano et al. (2000) changed slowly at $z > 0.5$ but increased much more rapidly starting at $z = 0.4$–0.5. While, the exact time at which the red-sequence assembly in clusters and the field cross and the time at which the S0 buildup becomes significant are not very well determined it is possible that the difference in redshift is real. If it is we may speculate that the ~ 0.7 Gyr difference in time between $z = 0.6$ and $z = 0.5$ may reflect an intrinsic delay between morphological transformation and the truncation of the SFR. As an example of such a scenario, the SFR may have been truncated during one pass through the cluster, while the morphological transformation may have required repeated cluster passages to build up the bulge (Christlein & Zabludoff 2004).

It is worth noting that Gilbank & Balogh (2008) compile many different measurements of $N_{\rm lum}/N_{\rm faint}$ in the field and cluster and find that $N_{\rm lum}/N_{\rm faint}$ evolves more quickly in the field than in the cluster. It is difficult to directly compare our results as we do not directly compare $N_{\rm lum}/N_{\rm faint}$ between the field and the cluster. We also find that the difference between the field and the cluster is most dramatic at red rest-frame wavelengths, whereas Gilbank & Balogh (2008) measured their $N_{\rm lum}/N_{\rm faint}$ in the rest-frame *V* band. It is also curious that the field $N_{\rm lum}/N_{\rm faint}$ in Gilbank & Balogh (2008) is observed to evolve quicker than for clusters but in DL07 and in this work, high-mass clusters are observed to evolve quicker in $N_{\rm lum}/N_{\rm faint}$ than low-mass clusters (see Section 5.2.2 for a discussion of these results). All we can say with some certainty is that the bright ends of the field

and cluster-measured LFs agree within our, admittedly, large error bars but that the faint ends do not, that this disagreement increases toward redder rest-frame bands, and that there seems to be a tentative indication that the direction of this disagreement changes over the EDisCS redshift range.

It is also interesting to discuss our results in light of similar cluster versus field comparisons in the local universe. Our finding that the faint-end slope in clusters is steeper than in the field at $0.4 < z < 0.6$ is in qualitative agreement with the local results using spectroscopically defined non-star-forming galaxies from 2dF (De Propris et al. 2003). However, De Propris et al. (2003) found that the clusters have a brighter $M^\star$ than the field, which may be inconsistent with our results at $0.4 < z < 0.6$. This may imply the presence of relative evolution in the bright end of the LF between the field and the cluster but it is important to keep in mind that our composite cluster LF is noisy at the bright end and that the local studies used spectroscopic techniques to identify galaxies with no star formation. Keeping this in mind, as we showed in Figure 5 the bright end of the measured EDisCS LFs is consistent with pure passive evolution, which would argue against a significant increase in the cluster red-sequence population at the luminous end toward lower redshift. One possible explanation is that red galaxies in the field are younger than those in clusters, and will therefore fade by a larger amount toward lower redshift. A useful check of this comes from fundamental plane studies. van der Wel et al. (2005) have shown that the evolution in M/L_B for massive galaxies in the cluster and field is $\Delta\ln(M/L_B) = (-1.12 \pm 0.06)z$ and $(-1.2 \pm 0.18)z$, respectively. These correspond to $\Delta M_B = (-1.22 \pm 0.06)z$ and $(-1.30 \pm 0.20)z$ for cluster and field galaxies, respectively. The lack of a difference between the LF evolution of red galaxies in the field and in clusters agrees with van Dokkum & van der Marel (2007) who have shown that massive ellipticals in clusters and the field have luminosity-weighted ages that are within 4.1% (≈0.4 Gyr) of each other. Gebhardt et al. (2003), however, find a ∼2 Gyr difference in the age of cluster and field ellipticals but the analysis of van Dokkum & van der Marel (2007) involves more sophisticated dynamical modeling and also corrects for selection effects such as, "progenitor bias" (van Dokkum & Franx 2001). In any case, this small difference between clusters and the field is not enough to explain the difference that we see with respect to De Propris et al. (2003). Another explanation must therefore be found to explain the apparent difference between the $M^\star$ in the field and clusters at intermediate- and low redshifts and what it implies for the relative evolution of bright ellipticals in these two extremes of environment. To better study the relative evolution of the bright end of the LF in the field and in the cluster it will be necessary to construct red-sequence LFs for much larger samples of clusters.

6.3. The Integrated Growth of the Red Sequence

In this subsection we explore the buildup of the total amount of light on the red sequence as the clusters evolve from $z \sim 0.4$–0.8 to $z \sim 0$. We start by measuring the total light on the cluster red sequence, $j_{\rm crs}$, by integrating the measured LFs in each cluster. We do this both at $r < 0.75$ Mpc and at $r < 0.5$ R_{200}, which scales with M_{200}. We present the results here for $r < 0.75$ Mpc. The choice of aperture for the $j_{\rm crs}$ computation is somewhat arbitrary, but we note that the results using $r < 0.5$ R_{200} are consistent with those computed using $r < 0.75$ Mpc but the trends are not as significant. In the left-hand column of Figure 11 we compare the total light on the red sequence

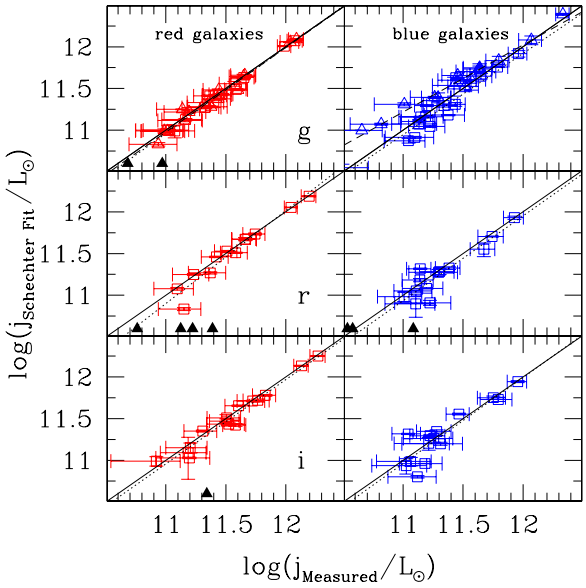

Figure 11. Comparison of j for galaxies in EDisCS clusters as computed by integrating the measured LF and by integrating the Schechter function fits to each cluster. The left-hand column is for red galaxies and the right-hand column is for blue galaxies. The open squares show the measured values with error bars on each quantity for the integral of LF_{zp} and the open triangles (only shown in the top panels—the g band) are for the integral of LF_{ss}. The vertical error bars are usually smaller than the points. The solid triangles on the bottom of each panel show the clusters with poor Schechter function fits. The solid diagonal line shows the one-to-one relation. The dotted and dashed lines show the least-squares fit to the data for LF_{zp} and LF_{ss}, respectively. The measured LFs seem to have converged for all the red LFs and for the blue LF_{zp}. We find some light missing for the faintest clusters when integrating LF_{ss}.

(A color version of this figure is available in the online journal.)

in each EDisCS cluster calculated both using the measured LF down to the magnitude limit of each cluster and using the complete integral of the best-fit Schechter function. The right-hand column is the same for blue galaxies, which we discuss later in this section. There are 3–4 clusters (with the number depending on the rest-frame bandpass) which have low measured luminosity and as a consequence also did not have well constrained Schechter fits (e.g., CL1227.9-1138 in Figure 4). For the rest of the clusters, however, the two measures of $j_{\rm crs}$ correlate very highly, with a mean offset of 3%–5% and a scatter of 9%. This demonstrates that our observations go deep enough to directly probe almost all of the light on the red sequence. Although the formal errors on the integral of the Schechter functions are much smaller than for the measured LF integrals, this is primarily because of our assumption of a parametric form for the LF and because we assume a well constrained faint-end slope, as determined by a fit to the composite LF in each redshift bin. To be as conservative as possible we therefore use $j_{\rm crs}$ derived from the measured LFs for the rest of this discussion. This has the added advantage of allowing us to include some of the lowest luminosity clusters that had poorly constrained Schechter function fits.

To perform a consistent comparison between low- and high-redshift clusters, and to mitigate any secondary dependences on cluster mass we compared our clusters to those in the local universe as a function of cluster mass. We calculate the mass, M_{200}, from the velocity dispersion following Finn et al. (2005):

$$M_{200} = 1.2 \times 10^{15} \left(\frac{\sigma}{1000 \text{ km s}^{-1}}\right)^3 \frac{1}{\sqrt{(\Omega_\Lambda + \Omega_M (1+z)^3)}} h_{100}^{-1} M_\odot. \quad (2)$$

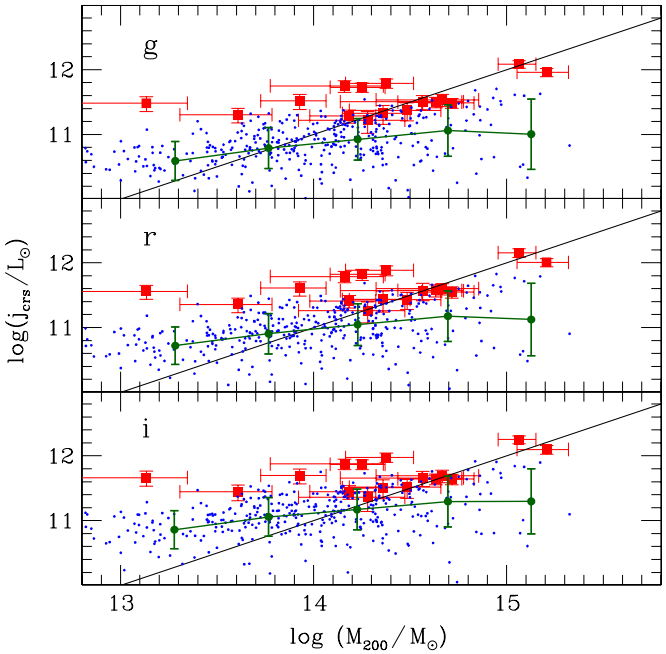

Figure 12. Comparison of M_{200} vs. j_{crs} in EDisCS clusters to that from clusters in the SDSS, in the rest-frame g, r, and i bands. The large solid squares show the EDisCS clusters, where the horizontal error bars show the 68% confidence intervals on M_{200} that stem from the uncertainty in the velocity dispersions. The small dots show the values for the SDSS clusters. The large circles are the geometric mean of the individual SDSS j_{crs} values in different mass bins. The solid vertical error bars on the SDSS points show the geometric standard deviation in each mass bin. The diagonal black line shows the slope that galaxies will lie on if they have constant j_{crs}/M_{200}. The SDSS clusters deviate significantly from this relation indicating a real trend of j_{crs}/M_{200} with M_{200}.

(A color version of this figure is available in the online journal.)

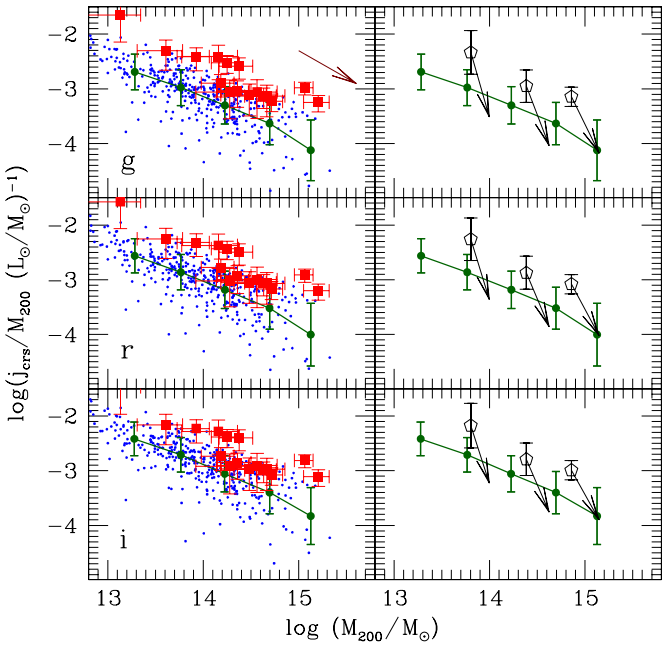

Figure 13. Comparison of j_{crs}/M_{200} vs. M_{200} for red-sequence galaxies in EDisCS clusters to that from clusters in the SDSS, in the rest-frame g, r, and i bands. (left column) The large solid squares show the EDisCS clusters, where the vertical and horizontal error bars show the 68% confidence intervals on j_{crs}/M_{200} and the errors in M_{200} that stem from the uncertainty in the velocity dispersions, respectively. The small dots show the values for the SDSS clusters. The large circles are the geometric mean of the individual SDSS j_{crs}/M_{200} values in different mass bins. The solid vertical error bars show the geometric standard deviation. Note that the errors in j_{crs}/M_{200} and M_{200} are correlated. The arrow in the upper-left panel demonstrates the change in j_{crs}/M_{200} that results from a factor of four change in M_{200}. (right column) The circles and error bars are the same as in the left column. The large open pentagons show the geometric mean of the EDisCS clusters in three mass bins chosen to contain roughly equal numbers of clusters, with the vertical error bars showing the geometric standard deviation for each value. The horizontal position of each pentagon is determined by the geometric mean of the masses for the EDisCS clusters in that mass bin. The arrows show the expected evolution from z_{clust} to $z = 0$ for a model in which the cluster mass increases by accretion but where no new galaxies are added to the red sequence and where those that are already present at the epoch of observation fade passively as SSPs with $z_f = 2$.

(A color version of this figure is available in the online journal.)

In Figure 12, we plot j_{crs} versus M_{200} for the EDisCS clusters and for the SDSS clusters. Even at a fixed mass in the SDSS sample there is significant scatter in integrated luminosity. This is intrinsic scatter in the cluster population as ∼95% of the SDSS clusters have lower than 20% error on the integrated luminosity. Although we have a large sample of SDSS clusters, the size of the local sample, especially at the massive end is the dominant uncertainty in the following analysis. The EDisCS clusters lie at brighter luminosities than the SDSS clusters at the same cluster mass. At a basic level this is expected because the red galaxies will fade as a function of time, moving the EDisCS points in the direction of the SDSS locus. We will quantify this evolution below.

It is also clear that the SDSS clusters deviate significantly from the one-to-one relation between M_{200} and j_{crs}(i.e., constant j_{crs}/M_{200}), which indicates that there is a residual dependence of j_{crs}/M_{200} on M_{200}. In this case, it appears that more massive clusters have a lower j_{crs}/M_{200} than less massive clusters. We have confirmed that this trend is not due to the uncertainties on the velocity dispersion for SDSS clusters. A similar deviation from the one-to-one relation between j_{crs} and M_{200} exists for the EDisCS clusters, such that clusters with low M_{200} are brighter than the one-to-one relation, but it is not clear how robust this is given the small numbers of very low mass clusters.

In Figure 13, we plot j_{crs}/M_{200} versus M_{200} for the EDisCS and SDSS clusters. In the left column we plot the individual values and in the right column we show the geometric mean j_{crs}/M_{200} of the EDisCS clusters in three mass bins and compare them to the SDSS clusters. The mass bins were chosen to contain approximately similar numbers of objects. We do not have enough clusters to bin both in mass and in redshift, but there is no dependence of sigma and redshift in our sample (see Figure 14) and a Spearman rank test gives only a 4% probability that the two values are correlated, i.e., our mass bins should not be affected by secondary correlation of cluster mass with redshift. Again, as in Figure 12 it is clear that the j_{crs}/M_{200} values for the EDisCS clusters are larger than for the SDSS clusters.

Even though the EDisCS clusters have higher j_{crs} for their M_{200} at $z \sim 0.6$ they must by definition evolve by $z \sim 0$ onto the local relation defined by the SDSS clusters. To explore what this constraint implies for the buildup of light (or mass) on the red sequence we have constructed a set of four toy models which we describe below. In all models we assume that two processes are universally present. First, the mass of clusters will grow via accretion of matter from the surrounding cosmic web. Second, the galaxies on the red sequence at the epoch of observation will only fade as a function of time, i.e., we assume that galaxies on the red sequence are passive and stay on the red sequence. We account for the growth of clusters by tracking the median growth in mass for clusters of a certain mass using the

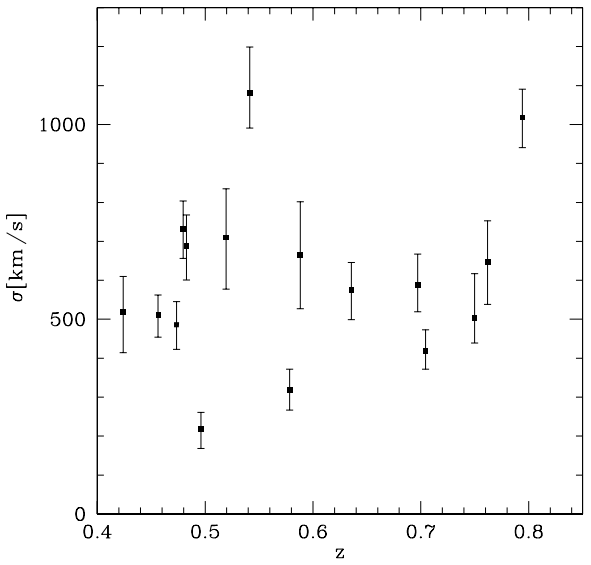

Figure 14. Velocity dispersions for our 16 clusters as a function of redshift. A Spearman Rank test gives a 4% probability that sigma is correlated with redshift.

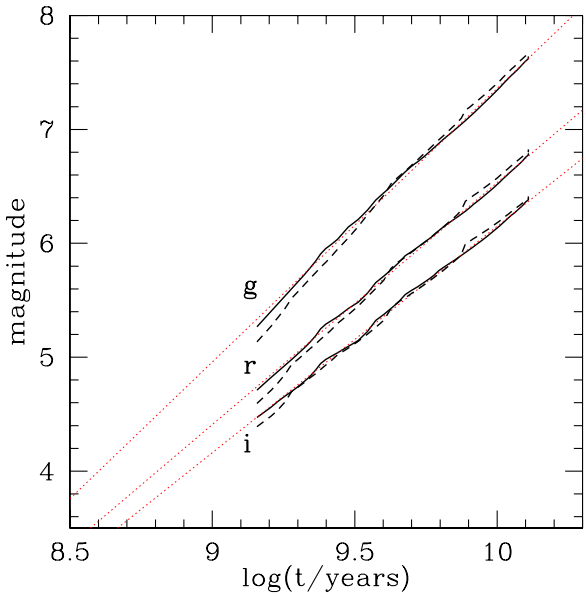

Figure 15. Fading as a function of time for simple stellar populations in the *g*, *r*, and *i* bands. The zero point of the *y*-axis is arbitrary. The thick solid line and thick dashed lines show the evolution in magnitude for SSP models with $Z = Z_{\odot}$ and 2.5 $Z_{\odot}$, respectively. The thin dotted line is the linear fit to the solar metallicity model. The 2.5 $Z_{\odot}$ model is brighter in the mean by 0.2–0.4 mag at these ages and we have subtracted out the difference to highlight the similar slopes. At $(t) > 1.4$ Gyr the fading in magnitude is well approximated by a linear relation in magnitude and log(t).

(A color version of this figure is available in the online journal.)

results of Wechsler et al. (2002) and Bullock et al. (2001).[24,25] To estimate the fading of cluster red-sequence galaxies, we fit a linear relation to the change of magnitude as a function of log(time) for each bandpass. In Figure 15 we show the fading in magnitude for models of two different metallicities(Bruzual & Charlot 2003). A linear fading of magnitude with log(age) is a very good approximation for SSPs with age$>$ 1.4 Gyr, as was shown originally by Tinsley (1980). Models with Z = $Z_{\odot}$ and 2.5 $Z_{\odot}$ differ in the amount of fading by < 0.13 mag over the 5.7 Gyr period from $z = 0.6$ to $z = 0$. We adopt the $Z = Z_{\odot}$ model but our results are insensitive to this choice. In tracking the fading stellar populations we evaluate whether galaxies fade below the absolute magnitude limit that we adopt for the SDSS. The first, simplest, and most unrealistic toy model is the one in which only mass is accreted but no light is added to the red sequence of the cluster. The light in the cluster therefore decreases by pure fading. In the right-hand panel of Figure 13, we demonstrate how this model would cause the EDisCS clusters to evolve from $z_{\rm clust}$ down to $z = 0$. This model results in predicted $j_{\rm crs}/M_{200}$ values at $z = 0$ that are too low compared to the SDSS. In Figure 16, we demonstrate this in another way by plotting the ratio of the predicted $z = 0$ *g*-band red-sequence luminosity, $j_{\rm crs,pred}$, to the observed SDSS red-sequence luminosity $j_{\rm crs,SDSS}$. From this figure it is clear that this first model results in predicted $z = 0$ luminosities that are too faint by a factor of $\sim$ 1–3 depending on the mass range, although formally the required mass growth implied in all three mass bins are consistent with each other. The red-sequence light in clusters must therefore grow by a similar factor from $z \sim 0.6$ to the $z \sim 0$. For clusters with $M_{200} < 10^{14.6}\mathcal{M}_{\odot}$ the required growth is a factor of 2.5–3. Because light and mass are proportional for red-sequence galaxies, this also implies that the stellar mass on the red sequence needs to therefore grow by a factor of 1–3 with a growth of 2.5–3 required at $M_{200} < 10^{14.6}\mathcal{M}_{\odot}$. That the largest implied growth may come from clusters of low to intermediate masses may be consistent with the results of Poggianti et al. (2006), who find that the star-forming fraction in clusters at $z < 0.8$ evolves most rapidly at intermediate cluster velocity dispersions (M_{200}) but evolves little at the highest velocity dispersions.

To explore different scenarios for how additional light (and stellar mass) may be added to the red sequence, we therefore consider a second model in which the cluster mass growth is accompanied by the accretion of stars with the same $M_{\rm tot}/L$ and its expected evolution, where $M_{\rm tot}/L$ is derived for each cluster individually using the total light in red-sequence cluster galaxies. In other words, this conservative model assumes that the only galaxies added to the red sequence are red-sequence field galaxies with the same ages and SFHs as cluster ellipticals and with the same proportion of light relative to the total mass. This model would be consistent, for example, with the very small age differences ($\sim$ 4%) found between cluster and field ellipticals by van Dokkum & van der Marel (2007). Assuming all galaxies that fall in to clusters at $z < 0.6$ end up on the red sequence at $z = 0$ this model represents the minimum amount of light that can be added to the cluster red sequence by accretion from the field. The results of this model are shown as the solid triangles in Figure 16. As expected these models yield higher predicted $z = 0$ luminosities for the EDisCS clusters, and are more consistent with the expectations for SDSS clusters.

It is interesting to discuss the predictions of this model in relation to the roughly factor of two growth in mass on the red sequence inferred from field studies (Bell et al. 2004; Faber et al. 2007; Brown et al. 2007). In interpreting this it is important to remember that the "field" surveys contain a range of environments, including moderate mass clusters for the largest surveys such as the NDWFS and extending to massive groups for the MUSYC, DEEP-2, and COMBO-17 surveys. The observed mass growth on the red sequence in field surveys represents the actual transformation of blue galaxies to red galaxies. Clusters, on the other hand, are growing their total mass by a factor of $\sim$ 2 at $z < 0.6$ and, at least partly, will be increasing the total

[24] We computed this using programs obtained from http://www.physics.uci.edu/~bullock/CVIR/

[25] Note that our highest mass clusters will evolve into objects that are so rare as not to be present at all in the SDSS C4 sample. This is also the fate of most of the numerous massive X-ray clusters at $z > 0.5$ that are found in the literature.

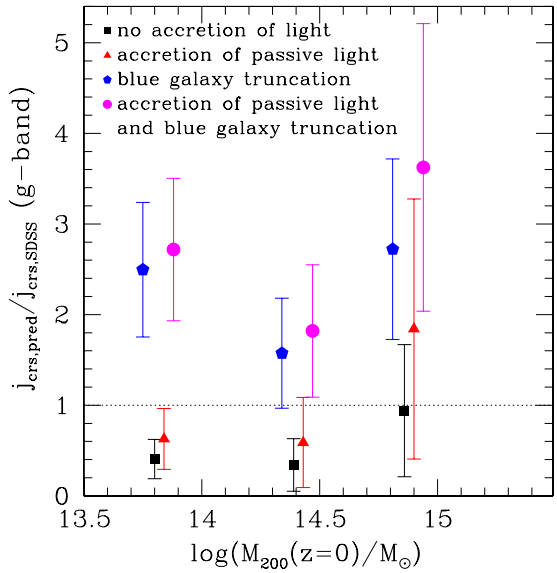

Figure 16. Ratio of the predicted red-sequence g-band luminosity, $j_{crs,pred}$, of EDisCS clusters at $z = 0$ to the measured j_{crs} from SDSS clusters, as a function of cluster mass. We show the predicted values for four toy models described in the text. The squares show a model in which only mass is added to the clusters but in which no new galaxies are added to the red sequence and those that exist at the epoch of observation evolve passively. The triangles show what happens when galaxies are added onto the red sequence with the same M_{tot}/L and its evolution as cluster galaxies. The pentagons show a model in which no additional red galaxies are accreted into the cluster but in which the blue galaxies in the clusters at $z = 0.6$ are assumed to have constant SFRs prior to the epoch of observation but subsequently have their SFR truncated and evolve passively thereafter. The circles show a model in which both the blue galaxies in the clusters are added to the red sequence and in which red passively evolving galaxies are accreted from the field. In all models, the error bars account for the dispersion in j_{crs} values in the EDisCS data. In the third and fourth models, the error bars also account for the different j_{bg} for different membership techniques and for the range of possible SFH. In each mass bin the points have been offset in mass for clarity.

(A color version of this figure is available in the online journal.)

amount of red light merely via the accretion of red galaxies from the field as in model 2 (above). Thus, the total increase that we infer in the mass on the red sequence is consistent with only a moderate additional transformation of blue to red galaxies. Nonetheless, our value for the required mass growth is still rather uncertain due to the significant intrinsic scatter both in the SDSS and EDisCS cluster j_{crs}/M_{200} values. Also, our middle and lowest mass bins ($M_{200} < 10^{14.6} \mathcal{M}_{\odot}$) imply a factor of $\sim$2.5−3 growth in the red-sequence stellar mass at $z < 0.8$, which may exceed the observed growth in the field and the expected total mass growth in clusters. As we show in Section 6.2, there is differential evolution in the shapes of the LFs in the field and clusters and this does imply that clusters evolve more rapidly in the number of galaxies on the red sequence. There is also evidence from Poggianti et al. (2006) that star-forming galaxies are being truncated preferentially in cluster environments but Finn et al. (2008) find that the decline in the SFRs of cluster galaxies at $z < 0.8$ is comparable to that in the field. While it is difficult to draw precise conclusions about the necessary mass transfer to the red sequence, it is clear that a pure passive fading of the cluster red sequence seen at $z = 0.4$–0.8 will result in clusters that are systematically too faint compared to those seen locally. Within the large uncertainties in the model predictions there is no significant trend with cluster mass, which is also true for each of the following models.

As a third model we calculate how much light is added to the EDisCS cluster red sequences by $z = 0$ by all of the blue galaxies in the clusters at $z = 0.4$–0.8, with no additional infall of red galaxies (pentagons; Figure 16). In calculating this estimate we take into account the uncertainties resulting from the differences between LF_{zp} and LF_{ss} that we determined in Section 4.5. Indeed, the total luminosity of blue galaxies in the g band, j_{bg}, determined from LF_{ss} ranges from 0.7 to 5.7 times larger than j_{bg} determined from LF_{zp}, with a median of 1.8, as calculated over all clusters. In addition, as is shown in the right-hand column of Figure 11 the blue galaxy g-band LF_{ss} has not converged completely for low-luminosity clusters due to the very steep faint-end slope. Nonetheless, for most of the clusters the missing light below our magnitude limit is small and j_{bg} as derived from LF_{ss} and LF_{zp} should still bracket the true value of j_{bg}. For every cluster we therefore use the mean of j_{bg} as determined from LF_{ss} and LF_{zp} and the values for the two methods as an indication of the uncertainty in j_{bg}. Because we can only calculate both LF_{ss} and LF_{zp} for the g band (see Section 4.1) we limit our analyses for the following models to that single bandpass. We then assume that the galaxies in each cluster have been forming stars constantly prior to the epoch of observation and that they have achieved solar metallicity by the time they are observed. We assume that they have $A_V = 1$, which corresponds to $A_g = 1.17$. Subsequent to observation we assume that these galaxies continue forming stars for 1 Gyr before abruptly ceasing their star formation and losing their dust. Except for the extra extinction, this is similar to the delayed truncation model of DL07 and is consistent with the evolution in the shape of the LF from $z = 0.8$ to 0. For every cluster, we calculate the expected luminosity contribution that these blue galaxies make to $j_{crs,pred}$ assuming that the galaxies were forming stars for 3–6 Gyr prior to observation. As we can see in Figure 16, this simple model overpredicts the amount of light on the red sequence in local clusters, especially so for the highest and lowest mass bins.

In reality, galaxies must be accreted onto the cluster over time and we therefore consider a fourth model in which both old ellipticals are accreted onto the cluster (model 2) and blue galaxies within the cluster are transformed (model 3). Being the sum of models 2 and 3, this fourth model naturally also overpredicts the predicted light in local clusters, by a factor of 1.8–3.6. In understanding why this last model overpredicts the local luminosity of clusters it is important first to remember that these models are in many ways very conservative in how much light is added to the red sequence by $z = 0$. The amount of mass that our clusters accrete is determined by ΛCDM and for this accreted mass we add the smallest possible amount of light to the red sequence by only accreting old galaxies at the same j_{crs}/M_{200} as the cluster. Accreting galaxies that are not as old as cluster ellipticals (e.g., blue galaxies) will increase the luminosities of the clusters by $z = 0$ with respect to our fourth model. In addition, there is little way to avoid the transformation of blue cluster galaxies at $z = 0.6$ to red and dead ones by $z = 0$ so our third model should also be valid. Because we accrete as little light as possible for the expected mass accretion, our fourth model can be thought of a lower limit on the amount of light added to the cluster (but see below). In light of these rather conservative assumptions it is perhaps puzzling that the simple model nonetheless produces too much cluster red sequence light at $z = 0$. As a note, the amount by which models 3 and 4 over predict local luminosities of clusters when computing j_{crs} at $r < 0.5\ R_{200}$ is consistent with, but not as large as when computing j_{crs} at $r < 0.75$ Mpc.

There are at least three possible resolutions to this apparent discrepancy. First, it may be that clusters accreted significant light in galaxies that never enter the red sequence by $z = 0$, i.e.,

from star-forming galaxies that have not had time to cease star formation and redden since they fell in. In our SDSS sample, we also computed the blue LF and find that $26 \pm 3\%$ of the total cluster light comes from galaxies bluer than the red sequence. Reducing the contribution to the final red-sequence luminosity by this amount corrects for our assumption that all accreted galaxies end up on the red sequence. This brings the fourth model into closer agreement with local cluster luminosities but still systematically overpredicts them.

A second possibility is that blue star-forming galaxies at $z = 0.6$ that enter the red sequence at $z = 0$ may still be dust enshrouded, lowering their total observed luminosity, something not encapsulated in our simple models. Indeed Wolf et al. (2005) find that roughly 1/3 of red-sequence galaxies in the Abell 901/902 supercluster are dusty star forming galaxies with $\langle A_V \rangle \approx 0.6$. If the same fraction of dusty red galaxies is present in all clusters, and under the simplifying assumption that the fraction of dusty galaxies is independent of galaxy luminosity, then this extinction changes the $j_{\rm crs}$ by a factor of 0.87. Taken alone this is obviously too small to make a significant contribution to reconciling model 4 with the local $j_{\rm crs}$ values. However, combining this with the amount of light from accreted galaxies that never make it onto the red sequence (see previous paragraph) would change $j_{\rm crs,pred}$ by a factor of 0.64, which still results in $j_{\rm crs,pred}$ values that are systematically a factor of 1.15–2.3 too high compared to local clusters, but are consistent within the 68% confidence limits.

Third, it is possible that a substantial fraction of stars / mass is in cluster components other than red-sequence galaxies, and is thus neglected in our measurement of the LF. For example, our LFs exclude the BCG and the intracluster light (ICL) which could harbor a significant fraction of the total stellar mass and may evolve differently than the red galaxies. Indeed, cluster galaxies are expected to sink to the cluster center and merge with the BCG ("cannibalism"; Ostriker & Tremaine 1975; White 1976), a phenomenon that has been observed in some low-redshift BCGs (Lauer 1988). Cannibalism may be especially relevant for the most massive cluster galaxies, for which the dynamical friction timescale is similar to the timescale we probe here (a few Gyrs). Hence, the extra mass in stars our toy model predicts could simply have been accreted onto the BCGs. However, Whiley et al. (2008) found that the properties of the EDisCS and SDSS BCGs are consistent with passive evolution since $z \sim 2$, implying no appreciable BCG mass growth. This result seems at odds with the factor of 3–4 mass growth of BCGs predicted by simulations (De Lucia & Blaizot 2007). One needs to keep in mind, however, that Whiley et al. (2008) considered only the central 37 kpc of each BCG and that any mass accreted in mergers must predominantly be accreted onto the envelope of the BCG and/or the ICL. This is also a viable possibility of explaining the discrepancy between our toy model prediction for the mass on the red sequence: rather than remaining in the galaxies we see in the cluster at $z \sim 0.6$, a significant fraction of old stars could be part of the ICL at $z = 0$, and are thus not accounted for in our LFs. There are various mechanisms by which cluster galaxies may get disrupted and lose their stars to the ICL: e.g., stripping due to tidal forces in the cluster gravitational field (Merritt 1984), or galaxy harassment (Farouki & Shapiro 1981; Moore et al. 1996). Indeed, the mass in the ICL has been measured in a number of low-redshift clusters, e.g., Mihos et al. (2005) detect ICL in the Virgo cluster and Gonzalez et al. (2007) find that the BCG+ICL contribute 20%–40% of the stellar light within R_{500} in clusters of the range in velocity dispersion we are considering here. This result is consistent with that of Zibetti et al. (2005), who found that the BCG+ICL contribute ~30% of the stellar light in stacked SDSS clusters. Furthermore, the color of the ICL is comparable to, or even slightly redder than, the total color of cluster galaxies Zibetti et al. (2005), implying that the ICL may have originated from red-sequence galaxies. Gonzalez et al. (2005) use the position angle and ellipticity for a set of lower redshift clusters to decompose the BCG and ICL and find that 80% of the light on average comes from the ICL. We do not know the ICL contribution in our high-redshift clusters, but if we assume that 20% of the light that would be on the red sequence at $z = 0$ ends up in the BCG+ICL this would move $j_{\rm crs,pred}$ for the fourth model even further into agreement with local values, implying that no new processes are needed to reconcile the red-sequence luminosities of clusters at $0.4 < z < 0.8$ with those locally.

Gonzalez et al. (2007) find that the fraction of light in the BCG+ICL decreases with increasing cluster velocity dispersion. Lin & Mohr (2004) measure a BCG magnitude that may include some ICL and they find that the luminosity fraction also decreases with increasing cluster mass. In both cases, the trends have a large scatter at velocity dispersions corresponding to our clusters and it is possible that a trend is present in our data but masked by the large scatter within our own sample. If such a trend exists, it is possible that the BCG and ICL build up at different rates and with a different response to the accretion history of the cluster. Hopefully more progress will be made with future high-resolution simulations of clusters in a cosmological context, and direct measurements of the high-redshift ICL.

7. SUMMARY AND CONCLUSIONS

In this paper, we have measured the rest-frame optical LFs for 16 clusters at $0.4 < z < 0.8$ that are drawn from the ESO Distant Cluster Survey (EDisCS). These clusters have a range in velocity dispersions and, in contrast to massive X-ray-selected high-redshift clusters, are the progenitors of "typical" clusters in the local universe (Milvang-Jensen et al. 2008).

We determined membership for our clusters using a photometric-redshift-based technique and one based on statistical background subtraction. From a detailed comparison of these two methods, we concluded that the LF could only be robustly determined for red-sequence galaxies and that the two methods resulted in very different $M^\star$ and α values for blue galaxies. We therefore focus on the LFs of red-sequence galaxies. We computed individual LFs for our clusters and composite LFs for the whole sample as well as for sample split into subsets by redshift at $z = 0.6$ and velocity dispersion at $\sigma = 600$ km s^{-1}. For the individual and composite LFs we fit Schechter functions, where we fixed the faint-end slope to the value determined from the fit to the composite of all EDisCS clusters in two different redshift bins.

As a low-redshift comparison sample we used a cluster catalog drawn from the SDSS and calculate the composite LF and its Schechter function fit as for the EDisCS clusters. When splitting the SDSS sample into bins of velocity dispersion we take into account the average mass growth in clusters as expected from numerical simulations. In this way we can compare clusters at high redshift to (representatives of) their likely descendants at low redshift, something that has not been possible with previous LF studies that either concentrated on very massive high-redshift clusters—whose descendants would be largely absent from local

volumes—or that had no velocity dispersion information for the clusters.

We measure significant evolution in the LF of cluster red-sequence galaxies at $z < 0.8$. In detail, the LFs show evolution in the bright end consistent with passive evolution but show a dramatic increase in the number of faint galaxies relative to bright ones toward lower redshifts, both within our own survey and when compared to the SDSS cluster sample. As a simple characterization of this evolution, we measure the ratio of luminous to faint galaxies as in De Lucia et al. (2007) and find similar results. We also measure the buildup of the red sequence as a more detailed function of magnitude and find tentative evidence for an evolving magnitude threshold brighter than which the LF is in place with respect to the local LF. It is not clear if this evolving magnitude threshold is in any way related to the evolving mass threshold seen in field samples, above which star formation is truncated (e.g., Bundy et al. 2006), or if it corresponds to a different cluster-related quenching mechanism. Indeed, the late buildup of the faint red sequence in clusters may also be related to the increase in the S0 fraction seen toward lower redshift.

We perform Schechter function fits to our LFs and find significant evolution in α but no evolution in $M^\star$, despite finding that the measured LFs at the bright end are consistent with passive evolution. This highlights the complications of using $M^\star$ as a measure of the evolution in the luminosity of the galaxy population as a whole when α is also simultaneously undergoing strong evolution. In our case, it must be that luminosities of the whole galaxy population are not evolving in lock step.

We split our sample into two bins of velocity dispersion and find only small differences in the detailed LFs, although we find the same result as DL07 that the ratio of luminous to faint galaxies is higher, and evolves more quickly, in clusters of higher velocity dispersion. We find indistinguishable luminous-to-faint ratios for SDSS clusters of different velocity dispersions, similar to that found by De Propris et al. (2003).

We looked for radial trends by examining the EDisCS LFs computed at $r < 0.75$ Mpc and $r < 0.5$ Mpc and find no difference in either $M^\star$ or α for red-sequence galaxies. This comparison, however, is uncertain as the two radial bins are highly correlated.

Using the field LF of red-sequence galaxies measured from the NDWFS (Brown et al. 2007) and MUSYC we compared our cluster LFs to the coeval field LF for similarly selected galaxies. At $0.6 < z < 0.8$ the field has more faint galaxies relative to bright ones than the clusters but at $0.4 < z < 0.6$ this has reversed, with the clusters having more faint galaxies than the field. This epoch is similar to that in which the buildup of the S0 population in clusters starts to become significant (Desai et al. 2007). Combined with the more rapid evolution of $N_{\rm lum}/N_{\rm faint}$ for high-velocity dispersion clusters, the different rates of evolution in the LFs imply that dense environments are more efficient than the field at adding galaxies to the red sequence at $z < 1$. These trends in the ratio of luminous to faint galaxies are reflected in the Schechter function fits. At both redshifts, the EDisCS LF has a more negative α than the field but a slightly fainter $M^\star$. While the former agrees with local cluster-field comparisons from 2dF, the latter disagrees. Discovering the cause of this discrepancy in the relative $M^\star$ values will require larger samples of clusters at intermediate redshift to increase the S/N of the LF at high luminosities.

To constrain different mechanisms for building up the red-sequence galaxy population we measure the total red-sequence light in the EDisCS and quantify its evolution with respect to clusters from SDSS. Clusters at high redshifts are overluminous compared to their likely local descendants. Once passive fading is accounted for it appears that the clusters are a factor of 1–3 underluminous compared to the local clusters that are their likely descendants. Since light traces stellar mass on the red sequence, this implies that the mass on the red sequence in clusters must grow by a factor of 1–3 at $z < 0.8$, with most of the growth occurring at the faint end of the LF where we directly witness strong evolution. This is a similar amount of growth in the red sequence as inferred from studies of the field LF (Bell et al. 2004; Faber et al. 2007; Brown et al. 2007) and indicates that the additional transformation of blue galaxies to red galaxies in clusters may be modest. However, due to the significant uncertainties we cannot determine if the total amount of mass added depends on cluster velocity dispersion. Evidence for environmental effects comes predominantly in the dependence of the shape evolution of the LF on cluster velocity dispersion and in differences between the cluster and field.

To explore what physical mechanisms may be driving the assembly of the red sequence, we explore a set of simple toy models that incorporate many of the processes that should add galaxies to the red sequence in clusters in a conservative manner. Accounting for all necessary processes we find that these models overpredict the light in local clusters. The model predictions can be reconciled with the data by a combination of three previously known processes: blue galaxies that have fallen in since $z < 0.6$ but are not on the red sequence at $z = 0$, attenuation of light on the red sequence by dust extinction, and the transfer of stars from galaxies to the diffuse cluster light via tidal stripping.

The results presented in this paper were only made possible with a large sample of clusters that span a range of redshift and velocity dispersion, that have accurately measured velocity dispersions, and that have deep multiwavelength photometry over a significant fraction of the virial radius. Our analysis was limited in large part by our reliance on photometric methods to isolate cluster members, and by the limited number of clusters in our sample. To improve upon the analysis several ingredients are needed. First, we need more clusters over a large range of mass, to confirm the mass-dependent assembly of the red sequence. Second, we need to move to larger radii so that we can probe out past R_{200} and thereby include many more galaxies in our sample. Third, we need increased spectroscopy of blue cluster members to allow a robust LF determination for galaxies of all colors. This last element would also be assisted if we had wide fields as we would then be able to do statistical background subtraction using "field" samples with identical photometry and roughly cospatial on the sky, thus bypassing many of the problems inherent in using external fields for background estimation.

G.R. thanks Casey Papovich, Jennifer Lotz, Daniel Eisenstein, and Mark Dickinson for useful discussions during the writing of this paper. G.R. also acknowledges the support of the Leo Goldberg Fellowship during his time at NOAO. The Dark Cosmology Centre is funded by the Danish National Research Foundation.

APPENDIX

REST-FRAME OPTICAL LUMINOSITY FUNCTIONS OF EDisCS CLUSTERS

Tables 5–10 give the LFs of 16 EDisCS clusters presented in Figure 4.

Table 5
Rest-frame g-Band LFs for EDisCS Clusters at $0.4 < z < 0.6$

M_g $M - 5\log h_{70}$	$\Phi_{\rm CL1018.8-1211}$	$\Phi_{\rm CL1037.9-1243}$	$\Phi_{\rm CL1059.2-1253}$	$\Phi_{\rm CL1138.2-1133}$	$\Phi_{\rm CL1202.7-1224}$	$\Phi_{\rm CL1232.5-1250}$	$\Phi_{\rm CL1301.7-1139}$	$\Phi_{\rm CL1353.0-1137}$	$\Phi_{\rm CL1411.1-1148}$	$\Phi_{\rm CL1420.3-1236}$
$-24.5 < M_g \leqslant -24.0$	< 2.00	< 2.00	< 2.00	< 2.00	< 2.00	< 2.00	< 2.00	< 2.00	< 2.00	< 2.00
$-24.0 < M_g \leqslant -23.5$	< 2.00	< 2.00	< 2.00	< 2.00	< 2.00	< 2.00	< 2.00	< 2.00	< 2.00	< 2.00
$-23.5 < M_g \leqslant -23.0$	< 2.00	< 2.00	< 2.00	< 2.00	< 2.00	< 2.00	< 2.00	< 2.00	< 2.00	< 2.00
$-23.0 < M_g \leqslant -22.5$	< 2.00	< 2.00	< 2.00	< 2.00	< 2.00	$1^{+2.41}_{-0.83}$	< 2.00	< 2.00	< 2.00	< 2.00
$-22.5 < M_g \leqslant -22.0$	< 2.00	< 2.00	$1^{+2.41}_{-0.83}$	< 2.00	$1^{+2.41}_{-0.83}$	$3^{+3.00}_{-1.63}$	< 2.00	$2^{+2.73}_{-1.29}$	$1^{+2.41}_{-0.83}$	$2^{+2.73}_{-1.29}$
$-22.0 < M_g \leqslant -21.5$	$1^{+2.41}_{-0.83}$	$1^{+2.41}_{-0.83}$	$5^{+3.45}_{-2.15}$	$1^{+2.41}_{-0.83}$	$1^{+2.41}_{-0.83}$	$4^{+3.24}_{-1.91}$	$1^{+2.41}_{-0.83}$	$1^{+2.41}_{-0.83}$	$2^{+2.73}_{-1.29}$	$1^{+2.41}_{-0.83}$
$-21.5 < M_g \leqslant -21.0$	$1^{+2.41}_{-0.83}$	$5^{+3.45}_{-2.15}$	$7^{+3.83}_{-2.58}$	$3^{+3.00}_{-1.63}$	< 2.00	$13^{+4.74}_{-3.55}$	$7^{+3.83}_{-2.58}$	$4^{+3.24}_{-1.91}$	$1^{+2.41}_{-0.83}$	$3^{+3.00}_{-1.63}$
$-21.0 < M_g \leqslant -20.5$	$3^{+3.00}_{-1.63}$	$3^{+3.00}_{-1.63}$	$10^{+4.32}_{-3.10}$	$10^{+4.32}_{-3.10}$	$1^{+2.41}_{-0.83}$	$16^{+5.12}_{-3.95}$	$9^{+4.16}_{-2.94}$	$6^{+3.65}_{-2.37}$	$6^{+3.65}_{-2.37}$	$7^{+3.83}_{-2.58}$
$-20.5 < M_g \leqslant -20.0$	$4^{+3.24}_{-1.91}$	$4^{+3.24}_{-1.91}$	$9^{+4.16}_{-2.94}$	$9^{+4.16}_{-2.94}$	$5^{+3.45}_{-2.15}$	$12^{+4.61}_{-3.41}$	$3^{+3.00}_{-1.63}$	$4^{+3.24}_{-1.91}$	$15^{+5.00}_{-3.83}$	$3^{+3.00}_{-1.63}$
$-20.0 < M_g \leqslant -19.5$	$14^{+4.87}_{-3.69}$	$2^{+2.73}_{-1.29}$	$9^{+4.16}_{-2.94}$	$6^{+3.65}_{-2.37}$	$6^{+3.65}_{-2.37}$	$12^{+4.61}_{-3.41}$	$6^{+3.65}_{-2.37}$	$6^{+3.65}_{-2.37}$	$6^{+3.65}_{-2.37}$	$5^{+3.45}_{-2.15}$
$-19.5 < M_g \leqslant -19.0$	$5^{+3.45}_{-2.15}$	$5^{+3.45}_{-2.15}$	$6^{+3.65}_{-2.37}$	$8^{+4.00}_{-2.76}$	$8^{+4.00}_{-2.76}$	$19^{+5.47}_{-4.32}$	$3^{+3.00}_{-1.63}$	$4^{+3.24}_{-1.91}$	$9^{+4.16}_{-2.94}$	$6^{+3.65}_{-2.37}$
$-19.0 < M_g \leqslant -18.5$	$7^{+3.83}_{-2.58}$	$4^{+3.24}_{-1.91}$	$8^{+4.00}_{-2.76}$	$6^{+3.65}_{-2.37}$	$2^{+2.73}_{-1.29}$	$12^{+4.61}_{-3.41}$	$6^{+3.65}_{-2.37}$	$4^{+3.24}_{-1.91}$	$8^{+4.00}_{-2.76}$	$3^{+3.00}_{-1.63}$
$-18.5 < M_g \leqslant -18.0$	$5^{+3.45}_{-2.15}$	$3^{+3.00}_{-1.63}$	$3^{+3.00}_{-1.63}$	$4^{+3.24}_{-1.91}$	$1^{+2.41}_{-0.83}$	$12^{+4.61}_{-3.41}$	$7^{+3.83}_{-2.58}$	$6^{+3.65}_{-2.37}$	$1^{+2.41}_{-0.83}$	$3^{+3.00}_{-1.63}$
$-18.0 < M_g \leqslant -17.5$	$4^{+3.24}_{-1.91}$	< 2.00	$5^{+3.45}_{-2.15}$	$5^{+3.45}_{-2.15}$	$2^{+2.73}_{-1.29}$	$24^{+6.00}_{-4.86}$	$11^{+4.46}_{-3.26}$	$4^{+3.24}_{-1.91}$	$3^{+3.00}_{-1.63}$	$4^{+3.24}_{-1.91}$
$-17.5 < M_g \leqslant -17.0$	$1^{+2.41}_{-0.83}$	$7^{+3.83}_{-2.58}$	$2^{+2.73}_{-1.29}$	$2^{+2.73}_{-1.29}$	$1^{+2.41}_{-0.83}$	...	$10^{+4.32}_{-3.10}$	...	...	$1^{+2.41}_{-0.83}$
$-17.0 < M_g \leqslant -16.5$	...	...	...	$2^{+2.73}_{-1.29}$	...	...	...	...	...	...

Note. Φ gives the number of galaxies per magnitude bin for each cluster and does not depend on h_{70}.

Table 6
Rest-frame g-Band LFs for EDisCS Clusters at $0.6 < z < 0.8$

M_g $M - 5\log h_{70}$	$\Phi_{\rm CL1040.7-1155}$	$\Phi_{\rm CL1054.4-1146}$	$\Phi_{\rm CL1054.7-1245}$	$\Phi_{\rm CL1216.8-1201}$	$\Phi_{\rm CL1227.9-1138}$	$\Phi_{\rm CL1354.2-1230}$
$-24.5 < M_g \leqslant -24.0$	< 2.00	< 2.00	< 2.00	< 2.00	< 2.00	< 2.00
$-24.0 < M_g \leqslant -23.5$	< 2.00	< 2.00	< 2.00	< 2.00	< 2.00	< 2.00
$-23.5 < M_g \leqslant -23.0$	< 2.00	< 2.00	< 2.00	< 2.00	< 2.00	< 2.00
$-23.0 < M_g \leqslant -22.5$	< 2.00	< 2.00	$1^{+2.41}_{-0.83}$	$3^{+3.00}_{-1.63}$	< 2.00	< 2.00
$-22.5 < M_g \leqslant -22.0$	$2^{+2.73}_{-1.29}$	$3^{+3.00}_{-1.63}$	$1^{+2.41}_{-0.83}$	$4^{+3.24}_{-1.91}$	< 2.00	$1^{+2.41}_{-0.83}$
$-22.0 < M_g \leqslant -21.5$	$3^{+3.00}_{-1.63}$	$3^{+3.00}_{-1.63}$	$3^{+3.00}_{-1.63}$	$13^{+4.74}_{-3.55}$	< 2.00	$3^{+3.00}_{-1.63}$
$-21.5 < M_g \leqslant -21.0$	$6^{+3.65}_{-2.37}$	$11^{+4.46}_{-3.26}$	$8^{+4.00}_{-2.76}$	$10^{+4.32}_{-3.10}$	$2^{+2.73}_{-1.29}$	$2^{+2.73}_{-1.29}$
$-21.0 < M_g \leqslant -20.5$	$3^{+3.00}_{-1.63}$	$8^{+4.00}_{-2.76}$	$10^{+4.32}_{-3.10}$	$14^{+4.87}_{-3.69}$	$3^{+3.00}_{-1.63}$	$3^{+3.00}_{-1.63}$
$-20.5 < M_g \leqslant -20.0$	$3^{+3.00}_{-1.63}$	$11^{+4.46}_{-3.26}$	$9^{+4.16}_{-2.94}$	$14^{+4.87}_{-3.69}$	$4^{+3.24}_{-1.91}$	$4^{+3.24}_{-1.91}$
$-20.0 < M_g \leqslant -19.5$	$2^{+2.73}_{-1.29}$	$10^{+4.32}_{-3.10}$	$7^{+3.83}_{-2.58}$	$8^{+4.00}_{-2.76}$	$2^{+2.73}_{-1.29}$	$3^{+3.00}_{-1.63}$
$-19.5 < M_g \leqslant -19.0$	< 2.00	$2^{+2.73}_{-1.29}$	$7^{+3.83}_{-2.58}$	$9^{+4.16}_{-2.94}$	< 2.00	$2^{+2.73}_{-1.29}$
$-19.0 < M_g \leqslant -18.5$	$1^{+2.41}_{-0.83}$	$7^{+3.83}_{-2.58}$	$8^{+4.00}_{-2.76}$	$10^{+4.32}_{-3.10}$	< 2.00	$1^{+2.41}_{-0.83}$
$-18.5 < M_g \leqslant -18.0$	< 2.00	$3^{+3.00}_{-1.63}$	$5^{+3.45}_{-2.15}$	$6^{+3.65}_{-2.37}$	< 2.00	< 2.00
$-18.0 < M_g \leqslant -17.5$	$2^{+2.73}_{-1.29}$	$3^{+3.00}_{-1.63}$	$9^{+4.16}_{-2.94}$	$8^{+4.00}_{-2.76}$	< 2.00	$3^{+3.00}_{-1.63}$
$-17.5 < M_g \leqslant -17.0$	...	...	...	...	$1^{+2.41}_{-0.83}$	...
$-17.0 < M_g \leqslant -16.5$	...	...	...	...	...	...

Notes. Φ gives the number of galaxies per magnitude bin for each cluster and does not depend on h_{70}. The LF for CL1227.9-1138 has been computed over $< 50\%$ of the full cluster area and so must be renormalized by the full area.

Table 7
Rest-frame r-Band LFs for EDisCS Clusters at $0.4 < z < 0.6$

M_r $M - 5\log h_{70}$	$\Phi_{\rm CL1018.8-1211}$	$\Phi_{\rm CL1037.9-1243}$	$\Phi_{\rm CL1059.2-1253}$	$\Phi_{\rm CL1138.2-1133}$	$\Phi_{\rm CL1202.7-1224}$	$\Phi_{\rm CL1232.5-1250}$	$\Phi_{\rm CL1301.7-1139}$	$\Phi_{\rm CL1353.0-1137}$	$\Phi_{\rm CL1411.1-1148}$	$\Phi_{\rm CL1420.3-1236}$
$-24.5 < M_r \leqslant -24.0$	< 2.00	< 2.00	< 2.00	< 2.00	< 2.00	< 2.00	< 2.00	< 2.00	< 2.00	< 2.00
$-24.0 < M_r \leqslant -23.5$	< 2.00	< 2.00	< 2.00	< 2.00	< 2.00	< 2.00	< 2.00	< 2.00	< 2.00	< 2.00
$-23.5 < M_r \leqslant -23.0$	< 2.00	< 2.00	$1^{+2.41}_{-0.83}$	< 2.00	< 2.00	$1^{+2.41}_{-0.83}$	< 2.00	$1^{+2.41}_{-0.83}$	< 2.00	< 2.00
$-23.0 < M_r \leqslant -22.5$	< 2.00	< 2.00	$2^{+2.73}_{-1.29}$	$1^{+2.41}_{-0.83}$	$1^{+2.41}_{-0.83}$	$4^{+3.24}_{-1.91}$	$1^{+2.41}_{-0.83}$	$1^{+2.41}_{-0.83}$	$1^{+2.41}_{-0.83}$	$2^{+2.73}_{-1.29}$
$-22.5 < M_r \leqslant -22.0$	$2^{+2.73}_{-1.29}$	$2^{+2.73}_{-1.29}$	$4^{+3.24}_{-1.91}$	< 2.00	$1^{+2.41}_{-0.83}$	$5^{+3.45}_{-2.15}$	$1^{+2.41}_{-0.83}$	$1^{+2.41}_{-0.83}$	$2^{+2.73}_{-1.29}$	$3^{+3.00}_{-1.63}$
$-22.0 < M_r \leqslant -21.5$	$3^{+3.00}_{-1.63}$	$4^{+3.24}_{-1.91}$	$10^{+4.32}_{-3.10}$	$3^{+3.00}_{-1.63}$	< 2.00	$13^{+4.74}_{-3.55}$	$8^{+4.00}_{-2.76}$	$7^{+3.83}_{-2.58}$	$5^{+3.45}_{-2.15}$	$4^{+3.24}_{-1.91}$
$-21.5 < M_r \leqslant -21.0$	$2^{+2.73}_{-1.29}$	$4^{+3.24}_{-1.91}$	$7^{+3.83}_{-2.58}$	$13^{+4.74}_{-3.55}$	$2^{+2.73}_{-1.29}$	$17^{+5.24}_{-4.08}$	$9^{+4.16}_{-2.94}$	$2^{+2.73}_{-1.29}$	$5^{+3.45}_{-2.15}$	$4^{+3.24}_{-1.91}$
$-21.0 < M_r \leqslant -20.5$	$7^{+3.83}_{-2.58}$	$3^{+3.00}_{-1.63}$	$10^{+4.32}_{-3.10}$	$8^{+4.00}_{-2.76}$	$5^{+3.45}_{-2.15}$	$10^{+4.32}_{-3.10}$	$2^{+2.73}_{-1.29}$	$5^{+3.45}_{-2.15}$	$13^{+4.74}_{-3.55}$	$3^{+3.00}_{-1.63}$
$-20.5 < M_r \leqslant -20.0$	$11^{+4.46}_{-3.26}$	$3^{+3.00}_{-1.63}$	$7^{+3.83}_{-2.58}$	$5^{+3.45}_{-2.15}$	$6^{+3.65}_{-2.37}$	$12^{+4.61}_{-3.41}$	$7^{+3.83}_{-2.58}$	$6^{+3.65}_{-2.37}$	$5^{+3.45}_{-2.15}$	$8^{+4.00}_{-2.76}$
$-20.0 < M_r \leqslant -19.5$	$3^{+3.00}_{-1.63}$	$4^{+3.24}_{-1.91}$	$6^{+3.65}_{-2.37}$	$8^{+4.00}_{-2.76}$	$8^{+4.00}_{-2.76}$	$19^{+5.47}_{-4.32}$	$2^{+2.73}_{-1.29}$	$4^{+3.24}_{-1.91}$	$10^{+4.32}_{-3.10}$	$4^{+3.24}_{-1.91}$
$-19.5 < M_r \leqslant -19.0$	$9^{+4.16}_{-2.94}$	$5^{+3.45}_{-2.15}$	$8^{+4.00}_{-2.76}$	$5^{+3.45}_{-2.15}$	$2^{+2.73}_{-1.29}$	$11^{+4.46}_{-3.26}$	$4^{+3.24}_{-1.91}$	$4^{+3.24}_{-1.91}$	$6^{+3.65}_{-2.37}$	$2^{+2.73}_{-1.29}$
$-19.0 < M_r \leqslant -18.5$	$4^{+3.24}_{-1.91}$	$2^{+2.73}_{-1.29}$	$3^{+3.00}_{-1.63}$	$4^{+3.24}_{-1.91}$	< 2.00	$17^{+5.24}_{-4.08}$	$7^{+3.83}_{-2.58}$	$3^{+3.00}_{-1.63}$	$2^{+2.73}_{-1.29}$	$3^{+3.00}_{-1.63}$
$-18.5 < M_r \leqslant -18.0$	$3^{+3.00}_{-1.63}$	$4^{+3.24}_{-1.91}$	$5^{+3.45}_{-2.15}$	$3^{+3.00}_{-1.63}$	$2^{+2.73}_{-1.29}$	$19^{+5.47}_{-4.32}$	$12^{+4.61}_{-3.41}$	$3^{+3.00}_{-1.63}$	$2^{+2.73}_{-1.29}$	$4^{+3.24}_{-1.91}$
$-18.0 < M_r \leqslant -17.5$	< 2.00	$2^{+2.73}_{-1.29}$	$2^{+2.73}_{-1.29}$	$5^{+3.45}_{-2.15}$	< 2.00	...	$10^{+4.32}_{-3.10}$	...	$1^{+2.41}_{-0.83}$	$1^{+2.41}_{-0.83}$
$-17.5 < M_r \leqslant -17.0$	...	...	...	$2^{+2.73}_{-1.29}$	$1^{+2.41}_{-0.83}$	...	...	...	...	...
$-17.0 < M_r \leqslant -16.5$	...	...	...	...	...	...	...	...	...	...

Note. Φ gives the number of galaxies per magnitude bin for each cluster and does not depend on h_{70}.

Table 8
Rest-frame r-Band LFs for EDisCS Clusters at $0.6 < z < 0.8$

M_r $M - 5\log h_{70}$	$\Phi_{\rm CL1040.7-1155}$	$\Phi_{\rm CL1054.4-1146}$	$\Phi_{\rm CL1054.7-1245}$	$\Phi_{\rm CL1216.8-1201}$	$\Phi_{\rm CL1227.9-1138}$	$\Phi_{\rm CL1354.2-1230}$
$-24.5 < M_r \leqslant -24.0$	< 2.00	< 2.00	< 2.00	< 2.00	< 2.00	< 2.00
$-24.0 < M_r \leqslant -23.5$	< 2.00	< 2.00	< 2.00	$1^{+2.41}_{-0.83}$	< 2.00	< 2.00
$-23.5 < M_r \leqslant -23.0$	< 2.00	$1^{+2.41}_{-0.83}$	$1^{+2.41}_{-0.83}$	$2^{+2.73}_{-1.29}$	< 2.00	< 2.00
$-23.0 < M_r \leqslant -22.5$	$4^{+3.24}_{-1.91}$	$2^{+2.73}_{-1.29}$	$1^{+2.41}_{-0.83}$	$8^{+4.00}_{-2.76}$	< 2.00	$1^{+2.41}_{-0.83}$
$-22.5 < M_r \leqslant -22.0$	$3^{+3.00}_{-1.63}$	$8^{+4.00}_{-2.76}$	$4^{+3.24}_{-1.91}$	$12^{+4.61}_{-3.41}$	$1^{+2.41}_{-0.83}$	$4^{+3.24}_{-1.91}$
$-22.0 < M_r \leqslant -21.5$	$5^{+3.45}_{-2.15}$	$9^{+4.16}_{-2.94}$	$9^{+4.16}_{-2.94}$	$10^{+4.32}_{-3.10}$	$2^{+2.73}_{-1.29}$	$2^{+2.73}_{-1.29}$
$-21.5 < M_r \leqslant -21.0$	$2^{+2.73}_{-1.29}$	$9^{+4.16}_{-2.94}$	$10^{+4.32}_{-3.10}$	$12^{+4.61}_{-3.41}$	$3^{+3.00}_{-1.63}$	$4^{+3.24}_{-1.91}$
$-21.0 < M_r \leqslant -20.5$	$4^{+3.24}_{-1.91}$	$10^{+4.32}_{-3.10}$	$8^{+4.00}_{-2.76}$	$15^{+5.00}_{-3.83}$	$4^{+3.24}_{-1.91}$	$2^{+2.73}_{-1.29}$
$-20.5 < M_r \leqslant -20.0$	$1^{+2.41}_{-0.83}$	$8^{+4.00}_{-2.76}$	$7^{+3.83}_{-2.58}$	$7^{+3.83}_{-2.58}$	$1^{+2.41}_{-0.83}$	$2^{+2.73}_{-1.29}$
$-20.0 < M_r \leqslant -19.5$	< 2.00	$2^{+2.73}_{-1.29}$	$6^{+3.65}_{-2.37}$	$8^{+4.00}_{-2.76}$	< 2.00	$3^{+3.00}_{-1.63}$
$-19.5 < M_r \leqslant -19.0$	$1^{+2.41}_{-0.83}$	$4^{+3.24}_{-1.91}$	$5^{+3.45}_{-2.15}$	$7^{+3.83}_{-2.58}$	< 2.00	$1^{+2.41}_{-0.83}$
$-19.0 < M_r \leqslant -18.5$	< 2.00	$4^{+3.24}_{-1.91}$	$4^{+3.24}_{-1.91}$	$4^{+3.24}_{-1.91}$	< 2.00	< 2.00
$-18.5 < M_r \leqslant -18.0$	$1^{+2.41}_{-0.83}$	< 2.00	...	...	< 2.00	...
$-18.0 < M_r \leqslant -17.5$	...	...	...	...	...	...
$-17.5 < M_r \leqslant -17.0$	...	...	...	...	...	...
$-17.0 < M_r \leqslant -16.5$	...	...	...	...	...	...

Notes. Φ gives the number of galaxies per magnitude bin for each cluster and does not depend on h_{70}. The LF for CL1227.9-1138 has been computed over $< 50\%$ of the full cluster area and so must be renormalized by the full area.

Table 9
Rest-frame i-Band LFs for EDisCS Clusters at $0.4 < z < 0.6$

M_i $M - 5\log h_{70}$	$\Phi_{\rm CL1018.8-1211}$	$\Phi_{\rm CL1037.9-1243}$	$\Phi_{\rm CL1059.2-1253}$	$\Phi_{\rm CL1138.2-1133}$	$\Phi_{\rm CL1202.7-1224}$	$\Phi_{\rm CL1232.5-1250}$	$\Phi_{\rm CL1301.7-1139}$	$\Phi_{\rm CL1353.0-1137}$	$\Phi_{\rm CL1411.1-1148}$	$\Phi_{\rm CL1420.3-1236}$
$-24.5 < M_i \leqslant -24.0$	< 2.00	< 2.00	< 2.00	< 2.00	< 2.00	< 2.00	< 2.00	< 2.00	< 2.00	< 2.00
$-24.0 < M_i \leqslant -23.5$	< 2.00	< 2.00	< 2.00	< 2.00	< 2.00	$1^{+2.41}_{-0.83}$	< 2.00	< 2.00	< 2.00	< 2.00
$-23.5 < M_i \leqslant -23.0$	< 2.00	< 2.00	$1^{+2.41}_{-0.83}$	< 2.00	$1^{+2.41}_{-0.83}$	$3^{+3.00}_{-1.63}$	< 2.00	$2^{+2.73}_{-1.29}$	$1^{+2.41}_{-0.83}$	$2^{+2.73}_{-1.29}$
$-23.0 < M_i \leqslant -22.5$	$1^{+2.41}_{-0.83}$	$1^{+2.41}_{-0.83}$	$4^{+3.24}_{-1.91}$	$1^{+2.41}_{-0.83}$	$1^{+2.41}_{-0.83}$	$3^{+3.00}_{-1.63}$	$1^{+2.41}_{-0.83}$	$1^{+2.41}_{-0.83}$	$2^{+2.73}_{-1.29}$	$2^{+2.73}_{-1.29}$
$-22.5 < M_i \leqslant -22.0$	$1^{+2.41}_{-0.83}$	$5^{+3.45}_{-2.15}$	$8^{+4.00}_{-2.76}$	$2^{+2.73}_{-1.29}$	< 2.00	$10^{+4.32}_{-3.10}$	$5^{+3.45}_{-2.15}$	$4^{+3.24}_{-1.91}$	$1^{+2.41}_{-0.83}$	$3^{+3.00}_{-1.63}$
$-22.0 < M_i \leqslant -21.5$	$3^{+3.00}_{-1.63}$	$2^{+2.73}_{-1.29}$	$7^{+3.83}_{-2.58}$	$12^{+4.61}_{-3.41}$	< 2.00	$17^{+5.24}_{-4.08}$	$11^{+4.46}_{-3.26}$	$5^{+3.45}_{-2.15}$	$6^{+3.65}_{-2.37}$	$5^{+3.45}_{-2.15}$
$-21.5 < M_i \leqslant -21.0$	$5^{+3.45}_{-2.15}$	$3^{+3.00}_{-1.63}$	$9^{+4.16}_{-2.94}$	$7^{+3.83}_{-2.58}$	$4^{+3.24}_{-1.91}$	$14^{+4.87}_{-3.69}$	$4^{+3.24}_{-1.91}$	$4^{+3.24}_{-1.91}$	$13^{+4.74}_{-3.55}$	$3^{+3.00}_{-1.63}$
$-21.0 < M_i \leqslant -20.5$	$10^{+4.32}_{-3.10}$	$4^{+3.24}_{-1.91}$	$8^{+4.00}_{-2.76}$	$5^{+3.45}_{-2.15}$	$7^{+3.83}_{-2.58}$	$7^{+3.83}_{-2.58}$	$4^{+3.24}_{-1.91}$	$5^{+3.45}_{-2.15}$	$6^{+3.65}_{-2.37}$	$3^{+3.00}_{-1.63}$
$-20.5 < M_i \leqslant -20.0$	$7^{+3.83}_{-2.58}$	$2^{+2.73}_{-1.29}$	$7^{+3.83}_{-2.58}$	$8^{+4.00}_{-2.76}$	$7^{+3.83}_{-2.58}$	$16^{+5.12}_{-3.95}$	$3^{+3.00}_{-1.63}$	$5^{+3.45}_{-2.15}$	$7^{+3.83}_{-2.58}$	$8^{+4.00}_{-2.76}$
$-20.0 < M_i \leqslant -19.5$	$7^{+3.83}_{-2.58}$	$5^{+3.45}_{-2.15}$	$8^{+4.00}_{-2.76}$	$5^{+3.45}_{-2.15}$	$4^{+3.24}_{-1.91}$	$17^{+5.24}_{-4.08}$	$6^{+3.65}_{-2.37}$	$3^{+3.00}_{-1.63}$	$9^{+4.16}_{-2.94}$	$4^{+3.24}_{-1.91}$
$-19.5 < M_i \leqslant -19.0$	$6^{+3.65}_{-2.37}$	$2^{+2.73}_{-1.29}$	$5^{+3.45}_{-2.15}$	$5^{+3.45}_{-2.15}$	$1^{+2.41}_{-0.83}$	$14^{+4.87}_{-3.69}$	$2^{+2.73}_{-1.29}$	$4^{+3.24}_{-1.91}$	$3^{+3.00}_{-1.63}$	$2^{+2.73}_{-1.29}$
$-19.0 < M_i \leqslant -18.5$	$4^{+3.24}_{-1.91}$	$3^{+3.00}_{-1.63}$	$5^{+3.45}_{-2.15}$	$3^{+3.00}_{-1.63}$	$2^{+2.73}_{-1.29}$	$11^{+4.46}_{-3.26}$	$12^{+4.61}_{-3.41}$	$4^{+3.24}_{-1.91}$	$1^{+2.41}_{-0.83}$	$4^{+3.24}_{-1.91}$
$-18.5 < M_i \leqslant -18.0$	< 2.00	< 2.00	$2^{+2.73}_{-1.29}$	$4^{+3.24}_{-1.91}$	< 2.00	$10^{+4.32}_{-3.10}$	$7^{+3.83}_{-2.58}$	...	$3^{+3.00}_{-1.63}$	$2^{+2.73}_{-1.29}$
$-18.0 < M_i \leqslant -17.5$	...	...	$1^{+2.41}_{-0.83}$	$2^{+2.73}_{-1.29}$	$1^{+2.41}_{-0.83}$	...	...	...	...	...
$-17.5 < M_i \leqslant -17.0$	...	...	...	...	...	...	...	...	...	...
$-17.0 < M_i \leqslant -16.5$	...	...	...	...	...	...	...	...	...	...

Note. Φ gives the number of galaxies per magnitude bin for each cluster and does not depend on h_{70}.

Table 10
Rest-frame i-Band LFs for EDisCS Clusters at $0.6 < z < 0.8$

M_i $M - 5\log h_{70}$	$\Phi_{\rm CL1040.7-1155}$	$\Phi_{\rm CL1054.4-1146}$	$\Phi_{\rm CL1054.7-1245}$	$\Phi_{\rm CL1216.8-1201}$	$\Phi_{\rm CL1227.9-1138}$	$\Phi_{\rm CL1354.2-1230}$
$-24.5 < M_i \leqslant -24.0$	< 2.00	< 2.00	< 2.00	< 2.00	< 2.00	< 2.00
$-24.0 < M_i \leqslant -23.5$	< 2.00	< 2.00	< 2.00	$3^{+3.00}_{-1.63}$	< 2.00	< 2.00
$-23.5 < M_i \leqslant -23.0$	$2^{+2.73}_{-1.29}$	$3^{+3.00}_{-1.63}$	$2^{+2.73}_{-1.29}$	$4^{+3.24}_{-1.91}$	< 2.00	$1^{+2.41}_{-0.83}$
$-23.0 < M_i \leqslant -22.5$	$3^{+3.00}_{-1.63}$	$4^{+3.24}_{-1.91}$	$3^{+3.00}_{-1.63}$	$13^{+4.74}_{-3.55}$	< 2.00	$2^{+2.73}_{-1.29}$
$-22.5 < M_i \leqslant -22.0$	$6^{+3.65}_{-2.37}$	$10^{+4.32}_{-3.10}$	$7^{+3.83}_{-2.58}$	$9^{+4.16}_{-2.94}$	$2^{+2.73}_{-1.29}$	$3^{+3.00}_{-1.63}$
$-22.0 < M_i \leqslant -21.5$	$3^{+3.00}_{-1.63}$	$10^{+4.32}_{-3.10}$	$9^{+4.16}_{-2.94}$	$13^{+4.74}_{-3.55}$	$3^{+3.00}_{-1.63}$	$2^{+2.73}_{-1.29}$
$-21.5 < M_i \leqslant -21.0$	$3^{+3.00}_{-1.63}$	$9^{+4.16}_{-2.94}$	$9^{+4.16}_{-2.94}$	$15^{+5.00}_{-3.83}$	$4^{+3.24}_{-1.91}$	$5^{+3.45}_{-2.15}$
$-21.0 < M_i \leqslant -20.5$	$2^{+2.73}_{-1.29}$	$9^{+4.16}_{-2.94}$	$7^{+3.83}_{-2.58}$	$9^{+4.16}_{-2.94}$	$2^{+2.73}_{-1.29}$	$1^{+2.41}_{-0.83}$
$-20.5 < M_i \leqslant -20.0$	< 2.00	$2^{+2.73}_{-1.29}$	$6^{+3.65}_{-2.37}$	$7^{+3.83}_{-2.58}$	< 2.00	$4^{+3.24}_{-1.91}$
$-20.0 < M_i \leqslant -19.5$	$1^{+2.41}_{-0.83}$	$5^{+3.45}_{-2.15}$	$5^{+3.45}_{-2.15}$	$6^{+3.65}_{-2.37}$	< 2.00	< 2.00
$-19.5 < M_i \leqslant -19.0$	< 2.00	$2^{+2.73}_{-1.29}$	$5^{+3.45}_{-2.15}$	$6^{+3.65}_{-2.37}$	< 2.00	$1^{+2.41}_{-0.83}$
$-19.0 < M_i \leqslant -18.5$	$1^{+2.41}_{-0.83}$	$3^{+3.00}_{-1.63}$	$5^{+3.45}_{-2.15}$	...	< 2.00	...
$-18.5 < M_i \leqslant -18.0$	...	...	...	...	< 2.00	...
$-18.0 < M_i \leqslant -17.5$	...	...	...	...	...	...
$-17.5 < M_i \leqslant -17.0$	...	...	...	...	...	...
$-17.0 < M_i \leqslant -16.5$	...	...	...	...	...	...

Notes. Φ gives the number of galaxies per magnitude bin for each cluster and does not depend on h_{70}. The LF for CL1227.9-1138 has been computed over $< 50\%$ of the full cluster area and so must be renormalized by the full area.

REFERENCES

Andreon, S. 2006, MNRAS, 369, 969
Andreon, S. 2008, MNRAS, 386, 1045
Aragón-Salamanca, A., Ellis, R. S., Couch, W. J., & Carter, D. 1993, MNRAS, 262, 764
Barger, A. J., et al. 1998, ApJ, 501, 522
Beers, T. C., Flynn, K., & Gebhardt, K. 1990, AJ, 100, 32
Bell, E. F., et al. 2004, ApJ, 608, 752
Bertin, E., & Arnouts, S. 1996, A& AS, 117, 393
Binggeli, B., Sandage, A., & Tammann, G. A. 1988, ARA&A, 26, 509
Blanton, M. R., et al. 2003, AJ, 125, 2348
Bolzonella, M., Miralles, J.-M., & Pelló, R. 2000, A&A, 363, 476
Bower, R. G. 1991, MNRAS, 248, 332
Bower, R. G., Kodama, T., & Terlevich, A. 1998, MNRAS, 299, 1193
Bower, R. G., Lucey, J. R., & Ellis, R. S. 1992, MNRAS, 254, 601
Brammer, G. B., van Dokkum, P. G., & Coppi, P. 2008, ApJ, 686, 1503
Brinchmann, J., Charlot, S., White, S. D. M., Tremonti, C., Kauffmann, G., Heckman, T., & Brinkmann, J. 2004, MNRAS, 351, 1151
Brown, M. J. I., Dey, A., Jannuzi, B. T., Brand, K., Benson, A. J., Brodwin, M., Croton, D. J., & Eisenhardt, P. R. 2007, ApJ, 654, 858
Brunner, R. J., & Lubin, L. M. 2000, AJ, 120, 2851
Bruzual, G., & Charlot, S. 2003, MNRAS, 344, 1000
Bullock, J. S., Kolatt, T. S., Sigad, Y., Somerville, R. S., Kravtsov, A. V., Klypin, A. A., Primack, J. R., & Dekel, A. 2001, MNRAS, 321, 559
Bundy, K., et al. 2006, ApJ, 651, 120
Christlein, D., & Zabludoff, A. I. 2004, ApJ, 616, 192
Cimatti, A., Daddi, E., & Renzini, A. 2006, A&A, 453, L29
Coil, A. L., et al. 2008, ApJ, 672, 153
Coleman, G. D., Wu, C. -C., & Weedman, D. W. 1980, ApJs, 43, 393
Colless, M. 1989, MNRAS, 237, 799
Croton, D. J., et al. 2006, MNRAS, 365, 11
De Lucia, G., & Blaizot, J. 2007, MNRAS, 375, 2
De Lucia, G., Springel, V., White, S. D. M., Croton, D., & Kauffmann, G. 2006, MNRAS, 366, 499
De Lucia, G., et al. 2004, ApJ, 610, L77
De Lucia, G., et al. 2007, MNRAS, 374, 809
De Propris, R., Stanford, S. A., Eisenhardt, P. R., Dickinson, M., & Elston, R. 1999, AJ, 118, 719
De Propris, R., Stanford, S. A., Eisenhardt, P. R., Holden, B. P., & Rosati, P. 2007, AJ, 133, 2209
De Propris, R., et al. 2003, MNRAS, 342, 725
de Vaucouleurs, G. 1961, ApJS, 5, 233
Desai, V., et al. 2007, ApJ, 660, 1151
Dressler, A. 1980, ApJ, 236, 351
Dressler, A., et al. 1997, ApJ, 490, 577
Faber, S. M., et al. 2007, ApJ, 665, 265
Farouki, R., & Shapiro, S. L. 1981, ApJ, 243, 32
Fasano, G., Poggianti, B. M., Couch, W. J., Bettoni, D., Kjærgaard, P., & Moles, M. 2000, ApJ, 542, 673
Fernández-Soto, A., Lanzetta, K. M., & Yahil, A. 1999, ApJ, 513, 34
Finn, R. A., Balogh, M. L., Zaritsky, D., Miller, C. J., & Nichol, R. C. 2008, ApJ, 679, 279
Finn, R. A., et al. 2005, ApJ, 630, 206
Folkes, S., et al. 1999, MNRAS, 308, 459
Gebhardt, K., et al. 2003, ApJ, 597, 239
Gehrels, N. 1986, ApJ, 303, 336
Gilbank, D. G., & Balogh, M. L. 2008, MNRAS, 385, L116
Gilbank, D. G., Yee, H. K. C., Ellingson, E., Gladders, M. D., Loh, Y.-S., Barrientos, L. F., & Barkhouse, W. A. 2008, ApJ, 673, 742
Gonzalez, A. H., Zabludoff, A. I., & Zaritsky, D. 2005, ApJ, 618, 195
Gonzalez, A. H., Zaritsky, D., Dalcanton, J. J., & Nelson, A. 2001, ApJS, 137, 117
Gonzalez, A. H., Zaritsky, D., & Zabludoff, A. I. 2007, ApJ, 666, 147
Goto, T., et al. 2005, ApJ, 621, 188
Halliday, C., et al. 2004, A&A, 427, 397
Hansen, S. M., Sheldon, E. S., Wechsler, R. H., & Koester, B. P. 2007, ApJ, submitted, arXiv:0710.3780
Häußler, B., et al. 2007, ApJS, 172, 615
Heidt, J., et al. 2003, A&A, 398, 49
Hogg, D. W., et al. 2002, AJ, 124, 646
Holden, B. P., Stanford, S. A., Eisenhardt, P., & Dickinson, M. 2004, AJ, 127, 2484
Hubble, E., & Humason, M. L. 1931, ApJ, 74, 43
Jørgensen, I., Chiboucas, K., Flint, K., Bergmann, M., Barr, J., & Davies, R. 2006, ApJ, 639, L9
Kodama, T., & Arimoto, N. 1997, A&A, 320, 41
Kodama, T., Smail, I., Nakata, F., Okamura, S., & Bower, R. G. 2001, ApJ, 562, L9
Kodama, T., et al. 2004, MNRAS, 350, 1005
Koo, D. C. 1986, ApJ, 311, 651
Kron, R. G. 1980, ApJS, 43, 305
Labbé, I., et al. 2003, AJ, 125, 1107
Lacey, C., & Cole, S. 1993, MNRAS, 262, 627
Lauer, T. R. 1988, ApJ, 325, 49
Lin, Y.-T., & Mohr, J. J. 2004, ApJ, 617, 879
Lotz, J. M., et al. 2008, ApJ, 672, 177
Marchesini, D., et al. 2007, ApJ, 656, 42
Marchesini, D., et al. 2009, ApJ, submitted, arXiv:0811.1773
McCracken, H. J., Le Fèvre, O., Brodwin, M., Foucaud, S., Lilly, S. J., Crampton, D., & Mellier, Y. 2001, A&A, 376, 756
Merritt, D. 1984, ApJ, 276, 26
Metcalfe, N., Shanks, T., Campos, A., McCracken, H. J., & Fong, R. 2001, MNRAS, 323, 795
Mihos, J. C., Harding, P., Feldmeier, J., & Morrison, H. 2005, ApJ, 631, L41
Miller, C. J., et al. 2005, AJ, 130, 968

Milvang-Jensen, B., et al. 2008, A&A, 482, 419
Moore, B., Katz, N., Lake, G., Dressler, A., & Oemler, A. 1996, Nature, 379, 613
Ostriker, J. P., & Tremaine, S. D. 1975, ApJ, 202, L113
Paolillo, M., Andreon, S., Longo, G., Puddu, E., Gal, R. R., Scaramella, R., Djorgovski, S. G., & de Carvalho, R. 2001, A&A, 367, 59
Pelló, R., et al. 2009, A&A, submitted
Pimbblet, K. A., Smail, I., Kodama, T., Couch, W. J., Edge, A. C., Zabludoff, A. I., & O'Hely, E. 2002, MNRAS, 331, 333
Poggianti, B. M., et al. 2006, ApJ, 642, 188
Popesso, P., Biviano, A., Böhringer, H., & Romaniello, M. 2006, A&A, 445, 29
Popesso, P., Böhringer, H., Romaniello, M., & Voges, W. 2005, A&A, 433, 415
Postman, M., et al. 2005, ApJ, 623, 721
Quadri, R., et al. 2007, AJ, 134, 1103
Rudnick, G., et al. 2001, AJ, 122, 2205
Rudnick, G., et al. 2003, ApJ, 599, 847
Salpeter, E. E. 1955, ApJ, 121, 161
Sanchez-Blazquez, P., et al. 2009, A&A, 499, 47
Scarlata, C., et al. 2007, ApJS, 172, 494
Schechter, P. 1976, ApJ, 203, 297
Schlegel, D. J., Finkbeiner, D. P., & Davis, M. 1998, ApJ, 500, 525
Simard, L., et al. 2002, ApJS, 142, 1
Simard, L., et al. 2009, A&A, submitted
Smith, G. P., Treu, T., Ellis, R. S., Moran, S. M., & Dressler, A. 2005, ApJ, 620, 78
Stanford, S. A., Eisenhardt, P. R., & Dickinson, M. 1998, ApJ, 492, 461
Stott, J. P., Smail, I., Edge, A. C., Ebeling, H., Smith, G. P., Kneib, J.-P., & Pimbblet, K. A. 2007, ApJ, 661, 95
Tanaka, M., Kodama, T., Arimoto, N., Okamura, S., Umetsu, K., Shimasaku, K., Tanaka, I., & Yamada, T. 2005, MNRAS, 362, 268
Tanaka, M., Kodama, T., Kajisawa, M., Bower, R., Demarco, R., Finoguenov, A., Lidman, C., & Rosati, P. 2007, MNRAS, 377, 1206
Taylor, E. N., et al. 2009, ApJ, 694, 1171
Thomas, D., Maraston, C., Bender, R., & Mendes de Oliveira, C. 2005, ApJ, 621, 673
Tinsley, B. M. 1980, Fundamentals of Cosmic Physics, 5, 287
Toft, S., Mainieri, V., Rosati, P., Lidman, C., Demarco, R., Nonino, M., & Stanford, S. A. 2004, A&A, 422, 29
Trager, S. C., Faber, S. M., & Dressler, A. 2008, MNRAS, 386, 715
Trager, S. C., Worthey, G., Faber, S. M., Burstein, D., & Gonzalez, J. J. 1998, ApJS, 116, 1
Tran, K.-V. H., Franx, M., Illingworth, G. D., van Dokkum, P., Kelson, D. D., Blakeslee, J. P., & Postman, M. 2007, ApJ, 661, 750
van der Wel, A., Franx, M., van Dokkum, P. G., Rix, H.-W., Illingworth, G. D., & Rosati, P. 2005, ApJ, 631, 145
van Dokkum, P. G., & Franx, M. 2001, ApJ, 553, 90
van Dokkum, P. G., & van der Marel, R. P. 2007, ApJ, 655, 30
Visvanathan, N., & Sandage, A. 1977, ApJ, 216, 214
von der Linden, A., Best, P. N., Kauffmann, G., & White, S. D. M. 2007, MNRAS, 379, 867
Wechsler, R. H., Bullock, J. S., Primack, J. R., Kravtsov, A. V., & Dekel, A. 2002, ApJ, 568, 52
Weinmann, S. M., van den Bosch, F. C., Yang, X., & Mo, H. J. 2006, MNRAS, 366, 2
Whiley, I. M., et al. 2008, MNRAS, 387, 1253
White, S. D. M. 1976, MNRAS, 177, 717
White, S. D. M., et al. 2005, A&A, 444, 365
Willmer, C. N. A., et al. 2006, ApJ, 647, 853
Wolf, C., Gray, M. E., & Meisenheimer, K. 2005, A&A, 443, 435
Wolf, C., et al. 2004, A&A, 421, 913
Wuyts, S., et al. 2008, ApJ, 682, 985
York, D. G., et al. 2000, AJ, 120, 1579
Zibetti, S., White, S. D. M., Schneider, D. P., & Brinkmann, J. 2005, MNRAS, 358, 949
Zucca, E., et al. 2006, A&A, 455, 879